

## The processes $\gamma\gamma \rightarrow ZH$ in SM and MSSM<sup>†</sup>.

G.J. Gounaris<sup>a</sup>, P.I. Porfyriadis<sup>a</sup> and F.M. Renard<sup>b</sup>

<sup>a</sup>Department of Theoretical Physics, Aristotle University of Thessaloniki,  
Gr-54006, Thessaloniki, Greece.

<sup>b</sup>Physique Mathématique et Théorique, UMR 5825  
Université Montpellier II, F-34095 Montpellier Cedex 5.

### Abstract

The process  $\gamma\gamma \rightarrow ZH$  first arises at the 1-loop level, and as such it provides remarkable tests of the structure of the electroweak Higgs sector. These tests are complementary to those in the gauge sector involving  $\gamma\gamma \rightarrow \gamma\gamma$ ,  $\gamma Z$ ,  $ZZ$ . We show that in the Standard Model (SM) where  $H = H_{SM}$ , as well as in the supersymmetric case where  $H = h^0$ ,  $H^0$  or  $A^0$ , observables exist (like *e.g.* the energy dependence, angular distribution, photon polarization dependence or final  $Z$  polarization) which present rather spectacular properties. Such properties involve strong threshold effects with steps, bumps or peaks, reflecting the type of Higgs and heavy quarks and chargino masses and couplings predicted by the SM and supersymmetric models.

---

<sup>†</sup>Partially supported by EU contract HPRN-CT-2000-00149.

# 1 Introduction

Photon-photon collisions have been recognized as being a remarkable place for testing the structure of the electroweak interactions at high energy, both in the gauge and in the Higgs sector [1]. These collisions should be experimentally feasible with the high intensity achievable through the laser backscattering procedure at a linear  $e^+e^-$  collider [2]. Many such studies [3] have been done in connection with the  $e^+e^-$  collider projects LC [4] and CLIC [5].

The significance of the photon-photon processes stems from the fact that they provide new tests of the fundamental interactions, which are often complementary to those achievable in direct  $e^+e^-$  collisions. These consist either in precise measurements sensitive to high order effects among standard and new particles, or in independent ways of producing new particles.

Of particular importance is the experimental study of the Higgs sector of the electroweak interactions, for which the Standard Model (SM) and the various extended models, like *e.g.* the Minimal Supersymmetric Standard Model (MSSM), give specific examples. In this respect, the basic photon-photon process is  $\gamma\gamma \rightarrow H$ , where  $H$  is a standard or a non standard neutral Higgs boson. This process arises at 1-loop and provides interesting tests of the Higgs boson couplings to the particles running inside the triangle loop; which could be the standard gauge bosons, leptons and quarks, as well as any new charged particles that might exist. New Higgs interactions could also be searched this way [6].

However the information obtained from  $\gamma\gamma \rightarrow H$  is restricted by the kinetic constraint  $s = m_H^2$ . To go beyond this, it is natural to look at the associate production  $\gamma\gamma \rightarrow ZH$  in which several observables sensitive to the dynamical contents, may be accessible. In SM or SUSY models, such processes first arise at the one loop level, contrary to the complementary process  $e^+e^- \rightarrow ZH$  which is dominated by the tree level contribution involving the  $ZZH$  coupling. So  $\gamma\gamma \rightarrow ZH$ , which has many similarities with the previously studied processes  $\gamma\gamma \rightarrow \gamma\gamma$ ,  $\gamma Z$ ,  $ZZ$  [7, 8, 9, 10, 11], should be sensitive to the quantum effects of the scalar sector and to the Higgs boson interactions with the particles running inside the loops.

In this paper we consider therefore the process  $\gamma\gamma \rightarrow ZH$  where  $H$  is either the standard Higgs boson  $H_{SM}$ , or a supersymmetric  $h^0, H^0$  or  $A^0$  state.

The dynamical contents at one loop is rather simple, but physically important. The generic form of the Feynman diagrams is depicted in Figs.1,2. It consists of triangle diagrams related to either an intermediate Higgs boson in the s-channel, or to a  $Z$  (plus Goldstone  $G^0$ ) exchange; and of box diagrams. These we classify as follows:

a) The diagrams with an intermediate Higgs boson in the s-channel only exist in the SUSY cases  $\gamma\gamma \rightarrow A^0 \rightarrow Zh^0$ ,  $ZH^0$  and  $\gamma\gamma \rightarrow H^0, h^0 \rightarrow ZA^0$ ; see Fig.1a for an  $A^0$  exchange and Figs.2a respectively. The related triangular loops describing  $\gamma\gamma \rightarrow H^0, h^0, A^0$  have been studied before and involve standard and supersymmetric bosonic and fermionic loops. These contributions are especially important in the  $\gamma\gamma \rightarrow A^0 \rightarrow Zh^0$  case for energies close to the  $A^0$  pole.

b) The diagrams with a  $(Z, G^0)$ -exchange involve the anomalous  $Z\gamma\gamma$  and  $G^0\gamma\gamma$  fermionic triangles, and the final  $(Z, G^0)ZH_{SM}$ ,  $(Z, G^0)Zh^0$  and  $(Z, G^0)ZH^0$  couplings; see<sup>1</sup> Fig.1a,b. This contribution vanishes when the  $Z$  is on shell, forcing the whole term to behave like a contact interaction with vanishing total angular momentum in the s-channel.

c) The box diagrams always involve fermionic loops; see Fig.1c-g, Fig.2b-f. No bosonic loop is allowed because of the charge conjugation properties of the boson couplings. In SM, the fermionic boxes only involve the standard lepton and quark contributions. The top quark contribution is predominant in this case, because of the two fermion mass factors imposed respectively on the amplitude by the Higgs couplings and the chirality violating nature of the process. In SUSY, for sufficient large  $\tan\beta$ , the importance of all quarks and leptons of the third family may be comparable; and we have in addition chargino boxes, involving either a single chargino running along the loop, or both charginos; (the later we call mixed chargino contribution).

The purpose of our study is to see how the various parts of the above contents reflect on the properties of the process  $\gamma\gamma \rightarrow ZH$ , and how this may be useful in testing the SM and MSSM models.

The contents of the paper is the following. In Section 2, we collect the elements of the SM and MSSM Lagrangian needed to compute the amplitudes in the four cases  $H = H_{SM}, h^0, H^0, A^0$ . The various couplings are collected in Appendix A. The helicity amplitudes generated by the various diagrams are explicitly given in analytic form in the Appendices B and C. In Section 3 we discuss the properties of the various observables of the process  $\gamma\gamma \rightarrow ZH$ . We consider the unpolarized and polarized  $\gamma\gamma$  cross sections, the  $ZH$  angular distributions and the final  $Z$  polarization. Several illustrations are given for SM and MSSM. A summary of the results is made in Section 4.

## 2 Dynamical characteristics of the process $\gamma\gamma \rightarrow ZH$

The generic set of the contributing diagrams is depicted in Fig.1a-g for the cases of  $\gamma\gamma \rightarrow Zh^0$  and  $\gamma\gamma \rightarrow ZH^0$ ; and in Fig.2a-f for the case of  $\gamma\gamma \rightarrow ZA^0$ . The SM case  $\gamma\gamma \rightarrow ZH_{SM}$  is obtained from Fig.1 by retaining only diagrams (1c) and (1b), together with the Goldstone involving part of (1a).

Boson loop contributions can only appear in the triangle diagram in Fig.2a, and involve  $W^\pm$  (plus goldstone and ghost) and charged Higgs, charged sleptons and squark lines. Their contributions have already been computed previously [11] and of course affects only  $\gamma\gamma \rightarrow ZA^0$ .

In all other diagrams, only internal fermion lines occur. These are the triangle diagrams Fig.1a,b and 2a, and the box diagrams 1c, 2b, involving internal standard charged fermion lines (leptons and quarks), as well as single chargino lines. Our conventions for the gauge boson couplings and the Yukawa couplings of the Higgs bosons ( $H^{SM}, h^0, H^0, A^0$ )

---

<sup>1</sup> Notice that there is no such contribution for  $ZA^0$  production.

to leptons and quarks are given in Appendix A. Note that the Yukawa couplings depend on the SUSY parameters  $\alpha$  and  $\beta$  of the Higgs sector, for which our conventions are as in [11].

The contribution of the third family of quarks and leptons, (essentially only the top quark in SM or low  $\tan\beta$  SUSY models), is strongly dominating the one from the lighter quarks and leptons. The reason is due to the presence of a factor  $m_f$  in the Yukawa couplings on the one hand; and due to the chirality flip along the fermionic lines of the loop, which introduces an additional  $m_f$  factor.

The  $Z, G^0$  exchange contribution corresponding to the diagrams (1b,a) has no  $Z$ -pole factor, and behaves like a contact interaction with the quantum numbers of a scalar exchange in the s-channel. It turns out that it is quite important in all SM or MSSM cases.

As already stated, the diagrams in Figs.1a-c, 2a,b also describe the contributions from a single chargino  $\tilde{\chi}^\pm$  running along the loop. Since the Yukawa-type couplings of the charginos involve no masses though, there is one power of fermion masses less, compared to the  $(t, b, \tau)$  case; see (A.8, A.9).

In addition to them though, we have the box diagrams Fig.1d-g, Fig.2c-f ( $j \neq i$ ) involving mixed chargino lines, due to the possibility of mixed  $Z\tilde{\chi}_1\tilde{\chi}_2$  and  $H\tilde{\chi}_1\tilde{\chi}_2$  couplings. The various unmixed and mixed couplings are defined in (A.3-A.5, A.8-A.10). They involve the full set of parameters of the SUSY chargino sector [11].

We have computed the helicity amplitudes  $F_{\lambda_1, \lambda_2, \lambda_Z}$  of the  $\gamma\gamma \rightarrow ZH$  process ( $H = H^{SM}, h^0, H^0, A^0$ ) generated by all these diagrams. They are explicitly given in Appendix B for the  $H_{SM}, h^0, H^0$  production cases, and in C for the  $A^0$  case<sup>2</sup>. The expressions are in terms of the Passarino-Veltman functions ( $C_0, D_0$ ) functions. As explained in the Appendices B and C, owing to the CP-invariance and Bose symmetry, there are only four "basic" amplitudes

$$F_{+++} \quad , \quad F_{+--} \quad , \quad F_{++0} \quad , \quad F_{+-0} \quad , \quad (1)$$

compare (B.7, C.5), from which all the other ones can be obtained. See also (B.8, B.4, C.2), as well as (B.9, C.6).

Before computing the various observables, we should point out certain important properties of the 1-loop contributions to the  $\gamma\gamma \rightarrow ZH$  helicity amplitudes.

Because of the scalar or pseudoscalar nature of the intermediate state, the triangle diagrams connected either to an intermediate Higgs boson or to an intermediate (virtual)  $Z, G^0$ -exchange, contribute only to the  $F_{\pm\pm 0}$  amplitude; compare the diagrams in Figs.1a,b, and 2a.

The (fermionic) box diagrams also favor the dominance of the  $F_{\pm\pm 0}$  amplitude. This is due to the chirality violating Higgs-fermion coupling on the one hand, and the Bose statistics for the two initial photons on the other. The chirality argument goes as follows. When the intermediate fermion-antifermion state is physical, chirality violation means  $\lambda_f = \lambda_{\bar{f}}$  for the fermion and antifermion helicities, which then favors  $\lambda_Z = 0$ ; i.e. dominance of longitudinal  $Z$  production. In addition to it, Eqs. (B.10, C.6), imposed by Bose

---

<sup>2</sup>For their definitions see (B.1, C.1)

symmetry, lead to the expectation that  $|F_{\pm\pm 0}| \gg |F_{\pm\mp 0}|$  at large angles.

We expect therefore that the whole contribution to the process  $\gamma\gamma \rightarrow ZH$  should be dominated by the  $F_{\pm\pm 0}$  amplitude. In a photon-photon collider this dominance of  $Z_L H$  production could be tested by looking at the decay distribution  $Z \rightarrow f\bar{f}$ , especially if one could study the charged lepton pairs. Moreover, the dominance of the  $\Delta\lambda = 0$  amplitudes should lead to a very simple form for the polarized photon-photon cross section

We next turn to the numerical results which indeed confirm the above expectations.

### 3 Results for the observables of the process $\gamma\gamma \rightarrow ZH$

In a  $\gamma\gamma$  Collider generated through Laser backscattering and employing various polarizations of laser photons and the  $e^\pm$  beams, we can a priori measure various types of "cross sections" through [8, 9, 10]

$$\frac{d\sigma}{d\tau d\cos\vartheta} = \frac{d\bar{L}_{\gamma\gamma}}{d\tau} \left\{ \frac{d\bar{\sigma}_0}{d\cos\vartheta} + \langle \xi_2 \xi'_2 \rangle \frac{d\bar{\sigma}_{22}}{d\cos\vartheta} + \langle \xi_3 \xi'_3 \rangle \frac{d\bar{\sigma}'_{33}}{d\cos\vartheta} \cos 2(\phi - \phi') + \dots \right\}, \quad (2)$$

where the dots stand for the various "cross section"  $\bar{\sigma}_j$  which do not involve the large  $F_{\pm\pm 0}(\gamma\gamma \rightarrow HZ)$  amplitudes. In (2),  $\tau = s/s_{ee}$  as usual, where  $s \equiv s_{\gamma\gamma}$  is defined in (B.2), while  $d\bar{L}_{\gamma\gamma}/d\tau$  describes the photon-photon luminosity per unit  $e^-e^+$  flux [1, 2, 3]. The Stokes parameters  $(\xi_2, \xi'_2)$ ,  $(\xi_3, \xi'_3)$  and  $(\phi, \phi')$  describe respectively the average helicities, transverse polarizations and azimuthal angles of the two backscattered photons [8, 9, 10]). In (2) there appear the "cross section" quantities

$$\frac{d\bar{\sigma}_0(\gamma\gamma \rightarrow ZH)}{d\cos\vartheta} \equiv \frac{\kappa}{64\pi s^2} \sum_{\lambda_Z} [ |F_{++\lambda_Z}|^2 + |F_{+-\lambda_Z}|^2 ], \quad (3)$$

$$\frac{d\bar{\sigma}_{22}(\gamma\gamma \rightarrow HZ)}{d\cos\vartheta} \equiv \frac{\kappa}{64\pi s^2} \sum_{\lambda_Z} [ |F_{++\lambda_Z}|^2 - |F_{+-\lambda_Z}|^2 ], \quad (4)$$

$$\frac{d\bar{\sigma}'_{33}(\gamma\gamma \rightarrow HZ)}{d\cos\vartheta} \equiv \frac{\kappa}{64\pi s^2} \sum_{\lambda_Z} \text{Re}[F_{++\lambda_Z} F_{--\lambda_Z}^*], \quad (5)$$

where  $\kappa$  is defined in (B.2) and it is related to the common  $Z$  and  $H$  momenta in their c.m. frame through (B.3); while  $\vartheta$  is the scattering angle in the same frame. Notice that  $\bar{\sigma}_0$  is the unpolarized  $\gamma\gamma \rightarrow ZH$  cross section. If only the  $F_{\pm\pm 0}$  amplitude were retained in (3-5), we would had gotten

$$\frac{d\bar{\sigma}_0}{d\cos\vartheta} \simeq \frac{d\bar{\sigma}_{22}}{d\cos\vartheta} \simeq \eta \frac{d\bar{\sigma}'_{33}}{d\cos\vartheta} \simeq \left( \frac{\kappa}{64\pi s^2} \right) |F_{++0}|^2, \quad (6)$$

with  $\eta = -1$  for  $H_{SM}, h^0, H^0$  and  $\eta = +1$  for  $A^0$  [8]; compare (B.4, C.2). These simple expressions imply very clean tests of the absence of unexpected contribution (beyond

SM or MSSM), to be performed using polarized laser and  $e^\pm$  beams. We now discuss separately the 4 cases of neutral Higgs boson production.

### The SM case.

In Fig.3a, we present the SM results for the  $\bar{\sigma}_0$ ,  $\bar{\sigma}_{22}$  "cross sections" integrated in the region  $\pi/3 \leq \vartheta \leq 2\pi/3$ , after summing over all  $Z$ -polarizations. We use<sup>3</sup>  $m_H = 130\text{GeV}$ . In Fig.3b the corresponding differential cross sections are given for the cases of  $Z$  production, either with all possible  $Z$ -polarizations summed, or with just  $\lambda_Z = 0$  retained.

As can be seen in Fig.3a,b, the differential and total "cross sections" for  $\bar{\sigma}_0$  and  $\bar{\sigma}_{22}$  are almost identical, and also equal to the corresponding cross sections for longitudinal  $Z$ -production. In fact we find that (6) is very accurately satisfied for all scattering angles, which just confirms that  $F_{\pm\pm 0}$  very strongly dominates all other amplitudes in the SM case.

In Fig.3a, a spectacular peak appears at the  $t\bar{t}$  threshold, which comes from the top quark contribution to the box-diagrams, as well as to the triangle ones inducing the anomalous  $Z, G^0$  contributions. It turns out that these contributions have similar sizes and interfere destructively at high energy, thus enforcing the fast decrease of the cross section. The angular distribution (see Fig.3b, paying attention to the scale in the y-axis) is, as expected from the relevant diagrams, rather flat. This may allow a clean detection of the  $ZH$  final state at large angles.

### The MSSM cases

We next turn to the supersymmetric cases of  $h^0$ ,  $H^0$ ,  $A^0$  production, exploring various sets of SUSY parameters. Two extreme typical sets with  $\tan\beta = 5$  (set A) and  $\tan\beta = 50$  (set B) are illustrated in Figs.4-6. The corresponding parameters, were calculated employing the unification condition

$$M_1 = \frac{5}{3} \tan^2 \theta_W M_2 \quad , \quad (7)$$

and using the HDECAY code [12]. The results for the physical masses and widths of the various Higgs bosons, the  $(\tilde{t}_1, \tilde{t}_2)$ -squarks and the charginos, are presented<sup>4</sup> in Table 1. In the calculations of the loops in all SUSY examples below, we just retain the quarks and leptons of the third family, the charginos, the gauge-bosons (together with their associated goldstone bosons and ghosts), and the charged Higgs and  $\tilde{t}_1, \tilde{t}_2$  bosons.

As one sees from the differential cross sections in these Figures, the dominance of  $Z_L$  production is true in all cases at the level of more than 98%. Also the equality of  $\bar{\sigma}_0$  with  $\bar{\sigma}_{22}$  (and also with  $\bar{\sigma}'_{33}$  not shown in this figure) is effective for  $h^0$  and  $A^0$  at more than 98%, and for  $H^0$  at more than 95%. We have checked that these results remain true as we go down in energy approaching the production threshold.

---

<sup>3</sup>Here, as well as in [11], we use  $\alpha = 1/137$ . This is to be contrasted to the results in [8, 9, 10] where  $\alpha = 1/128$  was used causing an increase of the overall magnitude of the various cross sections due to their  $\alpha^2$  factor.

<sup>4</sup>We have checked that the parameters in Sets A and B satisfy the requirements for the absence of charge or colour braking [13]

Table 1: SUSY Examples.  
(Particle masses and widths at the electroweak scale.)

$M_2 = 200\text{GeV}$ , $\mu = 300\text{GeV}$ , $M_{\tilde{f}} \simeq 1000\text{GeV}$		
	Set A	Set B
$\tan \beta$	5	50
$A_t = A_b = A_\tau$ (GeV)	2550	2500
$m_{\tilde{t}_1}$ (GeV)	781	780
$m_{\tilde{t}_2}$ (GeV)	1201	1201
$m_{\tilde{\chi}_1}$ (GeV)	170	180
$m_{\tilde{\chi}_2}$ (GeV)	337	333
$m_{h^0}$ (GeV)	119	126
$\Gamma_{h^0}$ (GeV)	0.0089	0.049
$m_{H^0}$ (GeV)	205	150
$\Gamma_{H^0}$ (GeV)	0.135	8.02
$m_{A^0}$ (GeV)	200	150
$\Gamma_{A^0}$ (GeV)	0.114	8.08
$m_{H^\pm}$ (GeV)	215	168

We now add specific comments for each of the supersymmetric Higgs bosons.

#### $h^0$ production.

As expected from the similarity of the basic  $h^0$  and  $H_{SM}$  couplings, this case is very close to the SM one. This is confirmed by the comparison of Figs.4 and 3. As is shown in Fig.4a,c, there is a strong dominance of the top quark box contribution and a large contribution from the anomalous  $Z, G^0$ -exchange diagrams, like in the SM case. For the case of Set B in particular (Fig.4c), the large  $\tan \beta$  value implies also appreciable  $b$ -quark and  $\tau$ -lepton contributions, which somewhat enhance the magnitude of the cross sections, compared to those of Set A. The chargino box contributes at most 10% of the cross section, and produces only small modifications around the two chargino thresholds. The angular distribution is also similar to the SM one.

#### $H^0$ production.

The results for the parameter Sets A and B of Table 1 are shown in Figs.5a-d. In this case there is no important top quark contribution to the box and to the anomalous  $Z, G^0$  diagrams, because the  $H^0 t\bar{t}$  coupling is weaker than the  $h^0 t\bar{t}$  one, and decreasing as  $\tan \beta$  increases [14]. This reduces considerably the  $H^0$  production cross sections, as compared to the  $h^0$ -ones. But at the same time, it allows for the appearance of very strong threshold effects due to the chargino boxes.

The shape and the size of these effects depend directly on the choice of the MSSM parameters controlling the size of the  $H\tilde{\chi}_i\tilde{\chi}_j$  couplings. The result is a rather complex addition of unmixed and mixed chargino contributions. Sets A and B illustrate how

one can get steps or peaks depending on the phase of the box amplitude (the relative size of the real and imaginary parts around the threshold) interfering with the real and imaginary parts of the  $t\bar{t}$  box. Steps are essentially due to the imaginary parts, while peaks are due to the real parts. So one has here a very nice way of testing the choice of MSSM parameters. The angular distribution is also rather flat but, depending on the set of SUSY parameters, one can see small violations of the  $\bar{\sigma}_0 = \bar{\sigma}_{22} = \bar{\sigma}'_{33}$  rule. So in this process the chargino contribution is very important and lead to several kinds of typical effects.

### $A^0$ production.

This  $A^0$ -production case, illustrated in Fig.6a-d, is somewhat different from the  $h^0$  and the  $H^0$  ones, because of the absence of anomalous  $Z, G^0$  contribution (there are no  $ZZA^0$  and  $G^0ZA^0$  couplings), and because the size of the  $A^0t\bar{t}$  and  $A^0\chi^+\chi^-$  couplings is different from the  $h^0$  or  $H^0$  ones. The contribution of the  $t$ -quark box is less pronounced than for  $h^0$ , but larger than for  $H^0$ . Correspondingly the chargino threshold effects have different shapes, i.e. steps or large bumps instead of narrow peaks. The sensitivity to the choice of MSSM parameters is still very large; compare the set A and B results illustrated in Fig.6a-d. The angular distributions of the various cross sections are always rather flat, but different curvatures appear, depending on the set of SUSY parameters. The overall magnitude of the  $\bar{\sigma}_0, \bar{\sigma}_{22}$  cross section in the  $A^0$  case tend to be considerably larger than those of the  $H^0$  one.

## 4 Conclusions

In this paper we have discussed the properties of the process  $\gamma\gamma \rightarrow ZH$  where  $H$  is either the SM Higgs boson  $H_{SM}$ , or any one of the three neutral supersymmetric Higgs bosons  $h^0, H^0, A^0$ . These processes only arise at the 1-loop level, involving triangle  $H - \gamma\gamma$  and  $Z, G^0 - \gamma\gamma$  diagrams, as well as  $\gamma\gamma ZH$ -box diagrams with internal charged fermionic lines ( $l, q, \chi_i^\pm$ ). We have shown how these contributions reflect in the  $\gamma\gamma \rightarrow ZH$  observables.

It appears that for all 4 cases, the helicity properties of the amplitudes are very simple. The final  $Z$  is almost always in the longitudinal state; *i.e.* for more than 98% of the cases. Moreover, all these processes occur for more than 95% of the times for initial photon-photon helicities in the  $\Delta\lambda = 0$  configuration. This implies that there is essentially only one amplitude contributing; namely the  $F_{\pm\pm 0}$  leading to

$$\sigma_0 \simeq \sigma_{22} \simeq \eta\sigma'_{33} \quad , \quad (8)$$

with  $\eta = -1$  for  $(H_{SM}, h^0, H^0)$ , and  $\eta = +1$  for  $A^0$ .

The  $ZH$  angular distribution is always rather flat, so that an important part of the events are produced at large angles, facilitating the detection.

The most spectacular properties concern the energy dependence of the cross section, which show strong threshold effects, due mainly to the fermionic box amplitudes. They are induced by the standard top quark and the supersymmetric  $\chi_i^\pm$  chargino contributions.



Depending on the type of the neutral Higgs boson produced and on the domain of MSSM parameter space, one can observe well pronounced threshold effects with steps, bumps or peaks. We have given typical illustrations in Figs.3-6 using two rather extreme sets of SUSY parameters.

We conclude by emphasizing that the neutral Higgs production processes considered here, provide remarkable tests of the structure of the electroweak interactions, which are complementary to those encountered in the gauge sector through studies of the  $\gamma\gamma \rightarrow \gamma\gamma$ ,  $\gamma Z$ ,  $ZZ$  transitions; and to the tests of the Higgs sector provided by  $\gamma\gamma \rightarrow H$ .

Although the cross sections seem rather small, several effects appear to be very spectacular. It appears therefore worthwhile that these processes are considered by the working groups, in order to study their observability at future high energy and high luminosity photon-photon colliders.

### **Acknowledgments.**

We are pleased to thank Abdelhak Djouadi for very informative discussions.

## Appendix A: The needed couplings in the Standard and SUSY models.

We generally give the couplings in SUSY models, specifying also the limit at which the SM ones are recovered. We use the same notation as in the Appendix of [11], giving here only the couplings needed in the present calculation. These consist of the photon- and Z-fermion ones determined by

$$\begin{aligned} \mathcal{L}_{Vff} = & -eQ_f A^\mu \bar{f} \gamma_\mu f - eZ^\mu \bar{f} (\gamma_\mu g_{vf}^Z - \gamma_\mu \gamma_5 g_{af}^Z) f , \\ & -eA^\mu \bar{\tilde{\chi}}_j \gamma_\mu \tilde{\chi}_j - eZ^\mu \bar{\tilde{\chi}}_j (\gamma_\mu g_{vj}^Z - \gamma_\mu \gamma_5 g_{aj}^Z) \tilde{\chi}_j \\ & -eZ^\mu [\bar{\tilde{\chi}}_1 (\gamma_\mu g_{v12}^Z - \gamma_\mu \gamma_5 g_{a12}^Z) \tilde{\chi}_2 + \text{h.c.}] , \end{aligned} \quad (\text{A.1})$$

where  $f$  is an ordinary quark or lepton and  $\tilde{\chi}_j$  ( $j = 1, 2$ ) are the two positively charged charginos. From this we have

$$g_{vf}^Z = \frac{t_3^f - 2Q_f s_W^2}{2s_W c_W} , \quad g_{af}^Z = \frac{t_3^f}{2s_W c_W} \quad (\text{A.2})$$

for the  $Zff$ -couplings, while Z-charginos ones are written as

$$\begin{aligned} g_{v1}^Z &= \frac{1}{2s_W c_W} \left( \frac{3}{2} - 2s_W^2 + \frac{1}{4} [\cos 2\phi_L + \cos 2\phi_R] \right) , \\ g_{a1}^Z &= -\frac{1}{8s_W c_W} [\cos 2\phi_L - \cos 2\phi_R] , \end{aligned} \quad (\text{A.3})$$

$$\begin{aligned} g_{v2}^Z &= \frac{1}{2s_W c_W} \left( \frac{3}{2} - 2s_W^2 - \frac{1}{4} [\cos 2\phi_L + \cos 2\phi_R] \right) , \\ g_{a2}^Z &= \frac{1}{8s_W c_W} [\cos 2\phi_L - \cos 2\phi_R] , \end{aligned} \quad (\text{A.4})$$

$$\begin{aligned} g_{v12}^Z &= g_{v21}^Z = -\frac{\text{Sign}(M_2)}{8s_W c_W} [\tilde{\mathcal{B}}_R \tilde{\Delta}_{12} \sin 2\phi_R + \tilde{\mathcal{B}}_L \sin 2\phi_L] , \\ g_{a12}^Z &= g_{a21}^Z = -\frac{\text{Sign}(M_2)}{8s_W c_W} [\tilde{\mathcal{B}}_R \tilde{\Delta}_{12} \sin 2\phi_R - \tilde{\mathcal{B}}_L \sin 2\phi_L] . \end{aligned} \quad (\text{A.5})$$

The sign quantities ( $\tilde{\Delta}_{12}$ ,  $\tilde{\mathcal{B}}_L$ ,  $\tilde{\mathcal{B}}_R$ ) in (A.5) are related to the definition of the chargino mixing angles, which is selected to always obey  $0 \leq \phi_L, \phi_R \leq \pi/2$ . They are given in Eqs.(A.35) in the Appendix of [11].

Also needed are the Yukawa couplings of the neutral Higgs bosons to the ordinary fermions and charginos determined by the effective Lagrangian

$$\begin{aligned} \mathcal{L}_{\text{Yukawa}} = & (g_{H^0 ff} H^0 + g_{h^0 ff} h^0) \bar{f} f + i\tilde{g}_{A^0 ff} A^0 \bar{f} \gamma_5 f + (g_j^{h^0} h^0 + g_j^{H^0} H^0) \bar{\tilde{\chi}}_j \tilde{\chi}_j \\ & + i\tilde{g}_j^{A^0} A^0 \bar{\tilde{\chi}}_j \gamma_5 \tilde{\chi}_j + [(g_{s12}^{h^0} h^0 + g_{s12}^{H^0} H^0 + g_{s12}^{A^0} A^0) \bar{\tilde{\chi}}_1 \tilde{\chi}_2 \\ & + (g_{p12}^{h^0} h^0 + g_{p12}^{H^0} H^0 + g_{p12}^{A^0} A^0) \bar{\tilde{\chi}}_1 \gamma_5 \tilde{\chi}_2 + \text{h.c.}] , \end{aligned} \quad (\text{A.6})$$

which for the quarks and leptons of the third family (the only ones needed to be retained) give

$$\begin{aligned}
g_{h^0 tt} &= -\frac{gm_t \cos \alpha}{2m_W \sin \beta} \quad , \quad g_{H^0 tt} = -\frac{gm_t \sin \alpha}{2m_W \sin \beta} \quad , \quad \tilde{g}_{A^0 tt} = \frac{gm_t}{2m_W} \cot \beta \\
g_{h^0 bb} &= \frac{gm_b \sin \alpha}{2m_W \cos \beta} \quad , \quad g_{H^0 bb} = -\frac{gm_b \cos \alpha}{2m_W \cos \beta} \quad , \quad \tilde{g}_{A^0 bb} = \frac{gm_b}{2m_W} \tan \beta \\
g_{h^0 \tau\tau} &= \frac{gm_\tau \sin \alpha}{2m_W \cos \beta} \quad , \quad g_{H^0 \tau\tau} = -\frac{gm_\tau \cos \alpha}{2m_W \cos \beta} \quad , \quad \tilde{g}_{A^0 \tau\tau} = \frac{gm_\tau}{2m_W} \tan \beta \quad . \quad (\text{A.7})
\end{aligned}$$

Parameters  $\alpha$ ,  $\beta$  are the usual SUSY Higgs sector angles. In the SM case, the couplings of  $H_{\text{SM}}$  should be identified with those of  $h^0$  by putting  $\alpha = \beta - \pi/2$ . Finally the Higgs-chargino couplings in (A.6) are given by

$$\begin{aligned}
g_1^{h^0} &= -\frac{g}{\sqrt{2}} \tilde{\Delta}_1 (-\cos \phi_R \sin \phi_L \sin \alpha \tilde{\mathcal{B}}_L + \sin \phi_R \cos \phi_L \cos \alpha \tilde{\mathcal{B}}_R) \quad , \\
g_1^{H^0} &= -\frac{g}{\sqrt{2}} \tilde{\Delta}_1 (\cos \phi_R \sin \phi_L \cos \alpha \tilde{\mathcal{B}}_L + \sin \phi_R \cos \phi_L \sin \alpha \tilde{\mathcal{B}}_R) \quad , \\
\tilde{g}_1^{A^0} &= -\frac{g}{\sqrt{2}} \tilde{\Delta}_1 (\cos \phi_R \sin \phi_L \sin \beta \tilde{\mathcal{B}}_L + \sin \phi_R \cos \phi_L \cos \beta \tilde{\mathcal{B}}_R) \quad , \quad (\text{A.8})
\end{aligned}$$

$$\begin{aligned}
g_2^{h^0} &= -\frac{g}{\sqrt{2}} \tilde{\Delta}_2 (-\cos \phi_R \sin \phi_L \cos \alpha \tilde{\mathcal{B}}_L + \sin \phi_R \cos \phi_L \sin \alpha \tilde{\mathcal{B}}_R) \quad , \\
g_2^{H^0} &= \frac{g}{\sqrt{2}} \tilde{\Delta}_2 (\cos \phi_R \sin \phi_L \sin \alpha \tilde{\mathcal{B}}_L + \sin \phi_R \cos \phi_L \cos \alpha \tilde{\mathcal{B}}_R) \quad , \\
\tilde{g}_2^{A^0} &= \frac{g}{\sqrt{2}} \tilde{\Delta}_2 (\cos \phi_R \sin \phi_L \cos \beta \tilde{\mathcal{B}}_L + \sin \phi_R \cos \phi_L \sin \beta \tilde{\mathcal{B}}_R) \quad , \quad (\text{A.9})
\end{aligned}$$

for the lighter and heavier chargino denoted as  $\tilde{\chi}_1$  and  $\tilde{\chi}_2$  respectively. As in the case of (A.5), the sign-quantities  $\tilde{\Delta}_1$ ,  $\tilde{\Delta}_2$ ,  $\tilde{\mathcal{B}}_L$ ,  $\tilde{\mathcal{B}}_R$  are also related to the chargino mixing and defined in (A.35) of the Appendix of [11]. Finally the mixed Higgs-chargino couplings are

$$\begin{aligned}
g_{s12}^{h^0} &= g_{s21}^{h^0} = \frac{g}{2\sqrt{2}} \text{Sign}(M_2) (\tilde{\Delta}_1 \cos \alpha - \tilde{\Delta}_2 \sin \alpha) [\tilde{\mathcal{B}}_{LR} \sin \phi_L \sin \phi_R - \tilde{\Delta}_{12} \cos \phi_L \cos \phi_R] \quad , \\
g_{p12}^{h^0} &= -g_{p21}^{h^0} = \frac{g}{2\sqrt{2}} \text{Sign}(M_2) (\tilde{\Delta}_1 \cos \alpha + \tilde{\Delta}_2 \sin \alpha) [\tilde{\mathcal{B}}_{LR} \sin \phi_L \sin \phi_R + \tilde{\Delta}_{12} \cos \phi_L \cos \phi_R] \quad , \\
g_{s12}^{H^0} &= g_{s21}^{H^0} = \frac{g}{2\sqrt{2}} \text{Sign}(M_2) (\tilde{\Delta}_1 \cos \alpha + \tilde{\Delta}_2 \sin \alpha) [-\cos \phi_L \cos \phi_R + \tilde{\Delta}_{12} \tilde{\mathcal{B}}_{LR} \sin \phi_L \sin \phi_R] \quad , \\
g_{p12}^{H^0} &= -g_{p21}^{H^0} = -\frac{g}{2\sqrt{2}} \text{Sign}(M_2) (\tilde{\Delta}_1 \cos \alpha - \tilde{\Delta}_2 \sin \alpha) [\cos \phi_L \cos \phi_R + \tilde{\Delta}_{12} \tilde{\mathcal{B}}_{LR} \sin \phi_L \sin \phi_R] \quad , \\
g_{s12}^{A^0} &= -g_{s21}^{A^0} \\
&= -i \frac{g}{2\sqrt{2}} \text{Sign}(M_2) (\tilde{\Delta}_1 \sin \beta - \tilde{\Delta}_2 \cos \beta) [\cos \phi_L \cos \phi_R + \tilde{\Delta}_{12} \tilde{\mathcal{B}}_{LR} \sin \phi_L \sin \phi_R] \quad , \\
g_{p12}^{A^0} &= g_{p21}^{A^0} \\
&= -i \frac{g}{2\sqrt{2}} \text{Sign}(M_2) (\tilde{\Delta}_1 \sin \beta + \tilde{\Delta}_2 \cos \beta) [\cos \phi_L \cos \phi_R - \tilde{\Delta}_{12} \tilde{\mathcal{B}}_{LR} \sin \phi_L \sin \phi_R] \quad . \quad (\text{A.10})
\end{aligned}$$

## Appendix B: The $\gamma\gamma \rightarrow Zh^0$ , $ZH^0$ , $ZH_{SM}$ helicity amplitudes.

The invariant helicity amplitudes for the process  $\gamma\gamma \rightarrow Zh^0$ , (or  $ZH^0$  or  $ZH_{SM}$ )

$$\gamma(k_1, \lambda_1)\gamma(k_2, \lambda_2) \rightarrow Z(q_1, \lambda_Z) h^0(q_2) \quad , \quad (\text{B.1})$$

are denoted as  $F_{\lambda_1\lambda_2\lambda_Z}(\kappa, t, u)$ , where the momenta and helicities of the incoming photons and outgoing  $Z$ 's are indicated in parentheses, and

$$\begin{aligned} s &= (k_1 + k_2)^2 \quad , \quad t = (k_1 - q_1)^2 \quad , \quad u = (k_1 - q_2)^2 \quad , \\ \kappa &= [s - (m - m_Z)^2]^{1/2}[s - (m + m_Z)^2]^{1/2} \quad . \end{aligned} \quad (\text{B.2})$$

Here  $m$  stands for the mass of the neutral Higgs boson in the final state. In the present case this is the mass of  $h^0$ , (or  $H^0$ ,  $H_{SM}$ ), but similar definitions will also be used for the  $A^0$  production case. Notice also that in the  $\gamma\gamma$  c.m. frame

$$|\vec{q}_1| = |\vec{q}_2| = \frac{\kappa}{2\sqrt{s}} \quad . \quad (\text{B.3})$$

The number of independent helicity amplitudes is reduced by various symmetries. Thus, if the only existing CP-violation is the usual one related to the standard part of the Yukawa forces; then at the 1-loop level the amplitudes should be CP invariant implying

$$F_{\lambda_1, \lambda_2, \lambda_Z}(\kappa, t, u) = -F_{-\lambda_1, -\lambda_2, -\lambda_Z}(\kappa, t, u)(-1)^{\lambda_Z} \quad , \quad (\text{B.4})$$

while Bose statistics imposes

$$F_{\lambda_1\lambda_2\lambda_Z}(\kappa, t, u) = F_{\lambda_2\lambda_1\lambda_Z}(\kappa, u, t)(-1)^{\lambda_Z} \quad , \quad (\text{B.5})$$

and the standard properties of the Z-polarization vectors give [10]

$$F_{\lambda_1, \lambda_2, \lambda_Z}(\kappa, t, u) = -F_{\lambda_1, \lambda_2, -\lambda_Z}(-\kappa, t, u)(-1)^{\lambda_Z} \quad . \quad (\text{B.6})$$

Therefore, there are only four independent helicity amplitudes which are taken as

$$F_{+++} \quad , \quad F_{+--} \quad , \quad F_{++0} \quad , \quad F_{+-0} \quad (\text{B.7})$$

and referred to below as "basic" amplitudes. The other amplitudes are determined by

$$\begin{aligned} F_{++-}(\kappa, t, u) &= F_{+++}(-\kappa, t, u) \quad , \\ F_{+-+}(\kappa, t, u) &= F_{+--}(-\kappa, t, u) \quad , \end{aligned} \quad (\text{B.8})$$

and (B.4). On the basis of (B.4-B.6), we also note that

$$F_{++0}(\kappa, t, u) = -F_{++0}(-\kappa, t, u) \quad , \quad (\text{B.9})$$

$$\begin{aligned} F_{+-0}(\kappa, t, u) &= -F_{+-0}(-\kappa, t, u) = -F_{-+0}(\kappa, t, u) \\ &= -F_{+-0}(\kappa, u, t) = F_{-+0}(\kappa, u, t) \quad . \end{aligned} \quad (\text{B.10})$$

At the 1-loop level, these amplitudes are expressed in terms of the  $C_0$  and  $D_0$  Passarino-Veltman functions [15], for which we follow the notation of [16] and the abbreviations<sup>5</sup>

$$C_0^{abc}(s) \equiv C_0(p_1, p_2; m_a, m_b, m_c) = C_0(0, 0, s; m_a, m_b, m_c) , \quad (\text{B.11})$$

$$C_h^{abc}(u) \equiv C_0(p_4, p_1; m_a, m_b, m_c) = C_0(m^2, 0, u; m_a, m_b, m_c) , \quad (\text{B.12})$$

$$C_Z^{abc}(u) \equiv C_0(p_3, p_2; m_a, m_b, m_c) = C_0(m_Z^2, 0, u; m_a, m_b, m_c) , \quad (\text{B.13})$$

$$C_h^{abc}(t) \equiv C_0(p_4, p_2; m_a, m_b, m_c) = C_0(m^2, 0, t; m_a, m_b, m_c) , \quad (\text{B.14})$$

$$C_Z^{abc}(t) \equiv C_0(p_3, p_1; m_a, m_b, m_c) = C_0(m_Z^2, 0, t; m_a, m_b, m_c) , \quad (\text{B.15})$$

$$C_{hZ}^{abc}(s) \equiv C_0(p_4, p_3; m_a, m_b, m_c) = C_0(m^2, m_Z^2, s; m_a, m_b, m_c) . \quad (\text{B.16})$$

Correspondingly for the  $D_0$ -functions, we note that

$$\begin{aligned} D_{hZ}^{abcd}(s, u) &\equiv D_0(p_4, p_3, p_2; m_a, m_b, m_c, m_d) = \\ &D_0(m^2, m_Z^2, 0, 0, s, u; m_a, m_b, m_c, m_d) , \end{aligned} \quad (\text{B.17})$$

$$\begin{aligned} D_{hZ}^{abcd}(s, t) &\equiv D_0(p_4, p_3, p_1; m_a, m_b, m_c, m_d) = \\ &D_0(m^2, m_Z^2, 0, 0, s, t; m_a, m_b, m_c, m_d) , \end{aligned} \quad (\text{B.18})$$

which for a common propagator mass simplify to

$$\begin{aligned} D_{hZ}^f(t, u) &\equiv D_0(p_4, p_2, p_3; m_f) = D_0(m^2, 0, m_Z^2, 0, t, u; m_f, m_f, m_f, m_f) \\ &= D_0(p_4, p_1, p_3; m_f) = D_0(m^2, 0, m_Z^2, 0, u, t; m_f, m_f, m_f, m_f) \\ &= D_0(p_3, p_2, p_4; m_f) = D_0(m_Z^2, 0, m^2, 0, u, t; m_f, m_f, m_f, m_f) . \end{aligned} \quad (\text{B.19})$$

In the same spirit, when *e.g.*  $m_a = m_b = m_c$ , the Passarino-Veltman C-functions are further abbreviated like in  $C_0^{abc}(s) \Rightarrow C_0^a(s)$ .

Correspondingly, for the case of two different propagator masses in a D-function we have

$$\begin{aligned} D_{hZ}^{abba}(t, u) &\equiv D_0(p_4, p_2, p_3; m_a, m_b, m_b, m_a) = D_0(p_4, p_1, p_3; m_b, m_a, m_a, m_b) \\ &= D_0(p_3, p_2, p_4; m_a, m_b, m_b, m_a) = D_0(p_3, p_1, p_4; m_b, m_a, m_a, m_b) \\ &= D_0(m^2, 0, m_Z^2, 0, t, u; m_a, m_b, m_b, m_a) = D_0(m^2, 0, m_Z^2, 0, u, t; m_b, m_a, m_a, m_b) \\ &= D_0(m_Z^2, 0, m^2, 0, u, t; m_a, m_b, m_b, m_a) \\ &= D_0(m_Z^2, 0, m^2, 0, t, u; m_b, m_a, m_a, m_b) . \end{aligned} \quad (\text{B.20})$$

Notice that (B.20) imply that

$$D_{hZ}^{abba}(t, u) = D_{hZ}^{baab}(u, t) . \quad (\text{B.21})$$

For the charginos boxes below, instead of the notation *e.g.*  $C_0^{\tilde{\chi}_2 \tilde{\chi}_1 \tilde{\chi}_1}(s)$ , we write  $C_0^{211}(s)$ .

---

<sup>5</sup>In (B.11-B.20), the momenta  $p_1 = k_1$ ,  $p_2 = k_2$  denoting the momenta of the photons, and  $p_3 = -q_1$ ,  $p_4 = -q_2$  being opposite to those of the final Z and  $h^0$ , are always taken as incoming; compare (B.1).

As in [10, 17, 11], it is convenient to define

$$\begin{aligned}
Y &= tu - m^2 m_Z^2 \quad , \quad s_h = s - m^2 \quad , \quad t_h = t - m^2 \quad , \quad u_h = u - m^2 \quad , \\
s_Z &= s - m_Z^2 \quad , \quad u_Z = u - m_Z^2 \quad , \quad t_Z = t - m_Z^2 \quad , 
\end{aligned} \tag{B.22}$$

$$\begin{aligned}
\tilde{F}^f(s, t, u) &= D_{hZ}^f(s, u) + D_{hZ}^f(s, t) + D_{hZ}^f(t, u) \quad , \\
E_1^f(s, u) &= u_h C_h^f(u) + u_Z C_Z^f(u) - su D_{hZ}^f(s, u) \quad , \\
E_2^f(t, u) &= u_h C_h^f(u) + u_Z C_Z^f(u) + t_h C_h^f(t) + t_Z C_Z^f(t) - Y D_{hZ}^f(t, u) \quad , \\
E_1^{ab}(s, u) &= u_h C_h^{baa}(u) + u_Z C_Z^{baa}(u) - su D_{hZ}^{abaa}(s, u) \quad , \\
E_2^{ab}(t, u) &= u_h C_h^{baa}(u) + u_Z C_Z^{baa}(u) + t_h C_h^{baa}(t) \\
&\quad + t_Z C_Z^{baa}(t) - Y D_{hZ}^{abba}(t, u) \quad . 
\end{aligned} \tag{B.23}$$

Notice that  $\tilde{F}^f(s, t, u)$ ,  $E_2^f(t, u)$  and  $E_1^{ab}(s, u)$ ,  $E_1^f(s, u)$  remain the same under interchanging  $m^2 \leftrightarrow m_Z^2$ ; while  $E_2^{ab}(t, u)$  remains the same under ( $m^2 \leftrightarrow m_Z^2$  and  $t \leftrightarrow u$ ).

**The  $A^0$ -pole contribution.** It only exists in SUSY models and it is described by the diagram in Fig.1a, in which only  $A^0$  exchange is considered. The fermion loop determining the  $\gamma\gamma A^0$  vertex of this diagram involves essentially only the  $t$  and  $b$  quarks, the  $\tau$ -leptons and the charginos. The only non-vanishing contribution from each of these fermions to the basic amplitudes appearing in (B.7), is for<sup>6</sup>

$$F_{++0}^{A^0 f\text{-pole}}(\gamma\gamma \rightarrow Zh^0) = -\frac{\alpha g Q_f^2 N_f^c}{2\pi m_W} \frac{\tilde{g}_{A^0 ff} \cos(\alpha - \beta)}{s - m_{A^0}^2 + im_{A^0} \Gamma_{A^0}} \kappa m_f s C_0^f(s) \quad , \tag{B.24}$$

where for quarks and leptons of the third family  $\tilde{g}_{A^0 ff}$  is given in (A.7); while for the two charginos the corresponding couplings are given by  $g_1^{A^0}$  and  $g_2^{A^0}$  in (A.8), (A.9) respectively. In (B.24)  $N_f^c$  is the colour factor, being 3 for quarks, and 1 for  $\tau$ 's and the charginos. As usually  $g = e/sw$ .

The corresponding contribution to the  $\gamma\gamma \rightarrow ZH^0$  process is given from (B.24) by replacing

$$\cos(\alpha - \beta) \Rightarrow -\sin(\beta - \alpha) \quad . \tag{B.25}$$

**The  $Z - G^0$ -exchange contribution.** It is described by the diagram in Fig.1b for the  $Z$ -exchange part, together with the neutral Goldstone exchange indicated in Fig.1a. In both cases the physical contribution only arises from the spin=0 part of the propagator exchanged in the s-channel, and there is no pole at  $m_Z^2$ . Notice that the diagram Fig.1b would also create a  $Z\gamma\gamma$  anomaly, which is being of course cancelled when a complete

---

<sup>6</sup>Notice that  $\alpha$  is used to describe both the fine structure constant, as well as the usual Higgs sector mixing angle. The discrimination among them in each case, should be easy though, from the structure of the formulae.

family of quarks and leptons or both charginos are included. The only non-vanishing contributions from these diagrams to the basic amplitudes of (B.7) are

$$F_{++0}^{tb\tau Z\text{-pole}}(\gamma\gamma \rightarrow Zh^0) = -\frac{\kappa\alpha^2 \sin(\beta - \alpha)}{s_W^2 c_W^2 m_Z^2} \left[ \frac{4m_t^2}{3} C_0^t(s) - \frac{m_b^2}{3} C_0^b(s) - m_\tau^2 C_0^\tau(s) \right] \quad (\text{B.26})$$

due to the mass differences among the quarks and leptons of the third family<sup>7</sup>, and

$$F_{++0}^{\tilde{\chi}_1 \tilde{\chi}_2 Z\text{-pole}}(\gamma\gamma \rightarrow Zh^0) = \frac{\kappa\alpha^2 \sin(\beta - \alpha)}{2s_W^2 c_W^2 m_Z^2} [\cos(2\phi_L) - \cos(2\phi_R)] \cdot \left[ m_{\tilde{\chi}_1}^2 C_0^{\tilde{\chi}_1}(s) - m_{\tilde{\chi}_2}^2 C_0^{\tilde{\chi}_2}(s) \right] \quad (\text{B.27})$$

from the two charginos.

The corresponding contribution to the  $\gamma\gamma \rightarrow ZH^0$  process is given from (B.26, B.27) by replacing

$$\sin(\beta - \alpha) \Rightarrow \cos(\beta - \alpha) \quad . \quad (\text{B.28})$$

**Single fermion box contribution.** The generic single fermion  $f$ -box diagram inducing this contribution, is shown in Fig.1c, where only the axial part of  $Z$  contributes. We write this contribution as

$$F_{\lambda_1 \lambda_2 \lambda_Z}^{f\text{-box}}(\gamma\gamma \rightarrow Zh^0 (H^0)) = r_f^{h^0(H^0)} \cdot A_{\lambda_1 \lambda_2 \lambda_Z}^{f\text{-box}}(H) \quad . \quad (\text{B.29})$$

The relevant couplings are collected in the coefficients, which for quarks or leptons are written as

$$\begin{aligned} r_f^{h^0} &= \frac{e^3}{(4\pi)^2} N_f^c Q_f^2 g_{af}^Z g_{h^0 ff} \quad , \\ r_f^{H^0} &= \frac{e^3}{(4\pi)^2} N_f^c Q_f^2 g_{af}^Z g_{H^0 ff} \quad , \end{aligned} \quad (\text{B.30})$$

(compare (A.2, A.7). The same expression also applies to the standard  $H_{SM}$  production process. Correspondingly, for a box with single chargino running along its sides, we have

$$r_f^{h^0(H^0)} = \frac{e^3}{(4\pi)^2} g_{aj}^Z g_j^{h^0(H^0)} \quad (\text{B.31})$$

with the couplings given in (A.3, A.4, A.8, A.9).

The  $A_{\lambda_1 \lambda_2 \lambda_Z}^{f\text{-box}}(H)$  terms in (B.29) are then given by

$$A_{+++}^{f\text{-box}}(H) = -\frac{\sqrt{2}m_f}{\kappa\sqrt{Y}s} \left\{ s(t-u)(t_h + u_h - \kappa)C_0^f(s) + 2u_h[t_h(t - \kappa) + m^2 u_Z + Y]C_h^f(u) \right.$$

---

<sup>7</sup>The contributions from the first two families is negligible due to their small masses.

$$\begin{aligned}
& -2u_Z[u_h(u - \kappa) + m^2 t_Z + Y]C_Z^f(u) + s(t_h + u_h - \kappa)(Y + u^2 - m^2 m_Z^2)D_{hZ}^f(s, u) \\
& - \frac{Y}{2}(t - u)(t_h + u_h - \kappa)D_{hZ}^f(t, u) - (t \leftrightarrow u) \Big\} , \tag{B.32}
\end{aligned}$$

$$\begin{aligned}
A_{+-}^{f\text{-box}}(H) = & -\frac{\sqrt{2}m_f}{\kappa\sqrt{sY^3}}(u - t + \kappa) \Big\{ s \left[ \kappa(t_h t_Z + u_h u_Z + Y) + s(u^2 - t^2) \right] C_0^f(s) \\
& + \kappa(Y + 2u_h u_Z)[u_h C_h^f(u) + u_Z C_Z^f(u)] + Y(u_Z + t_Z)[u_Z C_Z^f(u) - u_h C_h^f(u)] \\
& + s\kappa[t^2 + u^2 - 2m^2 m_Z^2 + (t - u)\kappa]C_{hZ}^f(s) + 2s(u^2 - m^2 m_Z^2)E_1^f(s, u) \\
& + 2sm_f^2 Y(\kappa + t - u)\tilde{F}^f(s, t, u) - \kappa s u [2u(u_h + t_Z) - Y]D_{hZ}^f(s, u) \\
& + \frac{Y^2 \kappa}{2} D_{hZ}^f(t, u) - (t \leftrightarrow u, \kappa \rightarrow -\kappa) \Big\} , \tag{B.33}
\end{aligned}$$

$$\begin{aligned}
A_{++0}^{f\text{-box}}(H) = & \frac{4m_f}{\kappa m_Z s} \Big\{ 2s^2(t + u)C_0^f(s) + [(t + u)(m^2 + m_Z^2) - 4m^2 m_Z^2]E_2^f(t, u) \\
& - 2m_f^2 s \kappa^2 \tilde{F}^f(s, t, u) - 2m^2 m_Z^2 s^2 [D_{hZ}^f(s, u) + D_{hZ}^f(s, t)] \Big\} , \tag{B.34}
\end{aligned}$$

$$\begin{aligned}
A_{+-0}^{f\text{-box}}(H) = & \frac{4m_f}{\kappa m_Z Y} \Big\{ (t - u)(t_Z + u_Z) \left[ s(t + u)C_0^f(s) - \kappa^2 C_{hZ}^f(s) - 2m_f^2 Y \tilde{F}^f(s, t, u) \right] \\
& + (t_Z + u_Z) \left[ (t^2 - m^2 m_Z^2)E_1^f(s, t) - (u^2 - m^2 m_Z^2)E_1^f(s, u) \right] \\
& + 2m_Z^2 Y \left[ u_h C_h^f(u) - t_h C_h^f(t) - u_Z C_Z^f(u) + t_Z C_Z^f(t) \right] \Big\} . \tag{B.35}
\end{aligned}$$

**Mixed chargino box involving axial Z coupling.** The generic form of the box diagrams giving this contribution is shown in Fig.1d,e. Their characteristic feature is that they involve the mixed axial Z-coupling of (A.5) and the  $g_{s12}^{h^0}, g_{s12}^{H^0}$  type of Higgs couplings appearing in (A.10). Notice that the diagrams of type (d) involve three identical chargino masses of one kind, and one of the other. On the contrary, the diagram of type (e) has two  $\tilde{\chi}_1$ -propagators and two of  $\tilde{\chi}_2$ . In analogy to (B.29), their contribution is written as

$$F_{\lambda_1 \lambda_2 \lambda_Z}^{Z_a \tilde{\chi}_1 \tilde{\chi}_2 \text{-box}}(\gamma\gamma \rightarrow Zh^0(H^0)) = r_{Z_a \chi_1 \chi_2}^{h^0(H^0)} \cdot A_{\lambda_1 \lambda_2 \lambda_Z}^{Z_a \tilde{\chi}_1 \tilde{\chi}_2 \text{-box}}(H) , \tag{B.36}$$

where the various couplings are absorbed in the coefficients

$$\begin{aligned}
r_{Z_a \chi_1 \chi_2}^{h^0} &= \frac{e^3}{(4\pi)^2} g_{a12}^Z g_{s12}^{h^0} , \\
r_{Z_a \chi_1 \chi_2}^{H^0} &= \frac{e^3}{(4\pi)^2} g_{a12}^Z g_{s12}^{H^0} , \tag{B.37}
\end{aligned}$$

for the  $h^0$  and  $H^0$  production respectively.



The  $A_{\lambda_1 \lambda_2 \lambda_Z}^{Z_a \tilde{\chi}_1 \tilde{\chi}_2 - \text{box}}$  terms in (B.36) are then given by

$$\begin{aligned}
A_{+++}^{Z_a \tilde{\chi}_1 \tilde{\chi}_2 - \text{box}}(H) = & -\frac{\sqrt{2}}{\kappa \sqrt{sY}} \left\{ \left\{ sm_{\tilde{\chi}_1}(t-u)(t_h + u_h - \kappa)C_0^{111}(s) \right. \right. \\
& + (m_{\tilde{\chi}_1} + m_{\tilde{\chi}_2}) \left[ u_h[t_h(t-\kappa) + m^2 u_Z + Y]C_h^{211}(u) - u_Z[u_h(u-\kappa) + m^2 t_Z + Y]C_Z^{211}(u) \right] \\
& + sm_{\tilde{\chi}_1}(t_h + u_h - \kappa)[Y + u^2 - m^2 m_Z^2 - (m_{\tilde{\chi}_1}^2 - m_{\tilde{\chi}_2}^2)(t-u)]D_{hZ}^{1211}(s, u) \\
& - \frac{(t-u)}{8}(m_{\tilde{\chi}_1} + m_{\tilde{\chi}_2})(t_h + u_h - \kappa)[s(m_{\tilde{\chi}_1} - m_{\tilde{\chi}_2})^2 + Y][D_{hZ}^{1221}(t, u) + D_{hZ}^{2112}(t, u)] \\
& - \frac{\kappa(m_{\tilde{\chi}_1} - m_{\tilde{\chi}_2})}{8}(t_h + u_h - \kappa)[s(m_{\tilde{\chi}_1} + m_{\tilde{\chi}_2})^2 + Y][D_{hZ}^{1221}(t, u) - D_{hZ}^{2112}(t, u)] \\
& \left. \left. - (t \leftrightarrow u) \right\} + (1 \leftrightarrow 2) \right\} , \tag{B.38}
\end{aligned}$$

$$\begin{aligned}
A_{+--}^{Z_a \tilde{\chi}_1 \tilde{\chi}_2 - \text{box}}(H) = & -\frac{(\kappa - t + u)}{\kappa \sqrt{2sY^3}} \left\{ \left[ s \left\{ s(m_{\tilde{\chi}_1} + m_{\tilde{\chi}_2})(u-t)[u+t+2(m_{\tilde{\chi}_1}^2 - m_{\tilde{\chi}_2}^2)] \right. \right. \right. \\
& + \kappa[m_{\tilde{\chi}_1}(t_Z t_h + u_Z u_h) - m_{\tilde{\chi}_2}s(t+u) - 2s(m_{\tilde{\chi}_1}^2 - m_{\tilde{\chi}_2}^2)(m_{\tilde{\chi}_1} + m_{\tilde{\chi}_2})] \left. \left. \right\} C_0^{111}(s) \right. \\
& + (m_{\tilde{\chi}_1} + m_{\tilde{\chi}_2}) \left\{ [2s(u^2 - m^2 m_Z^2) + \kappa(Y + 2u_h u_Z)][u_Z C_Z^{211}(u) + u_h C_h^{211}(u)] \right. \\
& + Y(u_Z + t_Z)[u_Z C_Z^{211}(u) - u_h C_h^{211}(u)] \left. \right\} + s\kappa(m_{\tilde{\chi}_1} + m_{\tilde{\chi}_2})[t^2 + u^2 - 2m^2 m_Z^2 \\
& + \kappa(t-u)]C_{hZ}^{121}(s) + 2s \left\{ (m_{\tilde{\chi}_1} + m_{\tilde{\chi}_2}) \left[ s(t-u)(m_{\tilde{\chi}_1}^2 - m_{\tilde{\chi}_2}^2)^2 - su(u^2 - m^2 m_Z^2) \right. \right. \\
& + 2m_{\tilde{\chi}_1}^2(t-u)Y + (m_{\tilde{\chi}_1}^2 - m_{\tilde{\chi}_2}^2)s[Y - 2(u^2 - m^2 m_Z^2)] \left. \left. \right\} \right. \\
& + \kappa \left\{ (m_{\tilde{\chi}_1} + m_{\tilde{\chi}_2})(m_{\tilde{\chi}_1}^2 - m_{\tilde{\chi}_2}^2)^2 s - 2u_Z u_h m_{\tilde{\chi}_1}(m_{\tilde{\chi}_1}^2 - m_{\tilde{\chi}_2}^2) + Y m_{\tilde{\chi}_1}(m_{\tilde{\chi}_1}^2 + m_{\tilde{\chi}_2}^2) \right. \\
& + m_{\tilde{\chi}_2} s u(u - 2m_{\tilde{\chi}_2}^2) - m_{\tilde{\chi}_1}(u + 2m_{\tilde{\chi}_1} m_{\tilde{\chi}_2})u_Z u_h \left. \right\} D_{hZ}^{1211}(s, u) \\
& + \frac{(m_{\tilde{\chi}_1} + m_{\tilde{\chi}_2})}{4} \left\{ 2s(t-u)[s(m_{\tilde{\chi}_1}^2 - m_{\tilde{\chi}_2}^2)^2 + (m_{\tilde{\chi}_1}^2 + m_{\tilde{\chi}_2}^2)Y] \right. \\
& + \kappa[2s(m_{\tilde{\chi}_1} - m_{\tilde{\chi}_2})^2 + Y][s(m_{\tilde{\chi}_1} + m_{\tilde{\chi}_2})^2 + Y] \left. \right\} [D_{hZ}^{1221}(t, u) + D_{hZ}^{2112}(t, u)] \\
& - \frac{(m_{\tilde{\chi}_1} - m_{\tilde{\chi}_2})Y}{4}(t_Z + u_Z)[s(m_{\tilde{\chi}_1} + m_{\tilde{\chi}_2})^2 + Y][D_{hZ}^{1221}(t, u) - D_{hZ}^{2112}(t, u)] \\
& \left. \left. - (t \leftrightarrow u, \kappa \rightarrow -\kappa) \right] + (1 \leftrightarrow 2) \right\} , \tag{B.39}
\end{aligned}$$

$$\begin{aligned}
A_{++0}^{Z_a \tilde{\chi}_1 \tilde{\chi}_2 - \text{box}}(H) = & \frac{2}{\kappa m_Z s} \left\{ 4m_{\tilde{\chi}_1} s^2(t+u)C_0^{111}(s) + (m_{\tilde{\chi}_1} + m_{\tilde{\chi}_2})[(t+u)(m^2 + m_Z^2) \right. \\
& - 4m^2 m_Z^2]E_2^{12}(t, u) - 2sm_{\tilde{\chi}_1} \left( m_{\tilde{\chi}_1} m_{\tilde{\chi}_2} \kappa^2 + 2sm^2 m_Z^2 + m_{\tilde{\chi}_1}^2 [(t+u)(m^2 + m_Z^2) - 4m^2 m_Z^2] \right. \\
& \left. \left. - sm_{\tilde{\chi}_2}^2(t+u) \right) [D_{hZ}^{1211}(s, u) + D_{hZ}^{1211}(s, t)] - (m_{\tilde{\chi}_1} + m_{\tilde{\chi}_2}) \left( s(m_{\tilde{\chi}_1}^2 + m_{\tilde{\chi}_2}^2) [(t+u)(m^2 + m_Z^2) \right. \right. \\
& \left. \left. - 4m^2 m_Z^2] - 2m_{\tilde{\chi}_1} m_{\tilde{\chi}_2} s^2(t+u) \right) D_{hZ}^{1221}(t, u) + (1 \leftrightarrow 2) \right\} , \tag{B.40}
\end{aligned}$$

$$\begin{aligned}
A_{+-0}^{Z_a\tilde{\chi}_1\tilde{\chi}_2\text{-box}}(H) &= \frac{(m_{\tilde{\chi}_1} + m_{\tilde{\chi}_2})}{\kappa m_Z Y} \left\{ \left\{ (t-u)(t_Z + u_Z) \left[ s[t+u + 2(m_{\tilde{\chi}_1}^2 - m_{\tilde{\chi}_2}^2)] C_0^{111}(s) \right. \right. \right. \\
&\quad \left. \left. \left. - \kappa^2 C_{hZ}^{121}(s) \right] - 2(t_Z + u_Z)(u^2 - m^2 m_Z^2) E_1^{12}(s, u) + 4m_Z^2 Y [u_h C_h^{211}(u) - u_Z C_Z^{211}(u)] \right. \right. \\
&\quad \left. \left. - 2(t_Z + u_Z) \left[ 2m_{\tilde{\chi}_1}^2 (t-u) Y + s(t-u)(m_{\tilde{\chi}_1}^2 - m_{\tilde{\chi}_2}^2)^2 \right. \right. \right. \\
&\quad \left. \left. \left. + s(m_{\tilde{\chi}_1}^2 - m_{\tilde{\chi}_2}^2) [Y - 2(u^2 - m^2 m_Z^2)] \right] D_{hZ}^{1211}(s, u) - \frac{(t-u)}{2} (t_Z + u_Z) [s(m_{\tilde{\chi}_1}^2 - m_{\tilde{\chi}_2}^2)^2 \right. \right. \\
&\quad \left. \left. + Y(m_{\tilde{\chi}_1}^2 + m_{\tilde{\chi}_2}^2)] [D_{hZ}^{1221}(t, u) + D_{hZ}^{2112}(t, u)] \right. \right. \\
&\quad \left. \left. + \frac{m_{\tilde{\chi}_1} - m_{\tilde{\chi}_2}}{m_{\tilde{\chi}_1} + m_{\tilde{\chi}_2}} m_Z^2 Y [Y + s(m_{\tilde{\chi}_1} + m_{\tilde{\chi}_2})^2] [D_{hZ}^{1221}(t, u) - D_{hZ}^{2112}(t, u)] \right. \right. \\
&\quad \left. \left. - (t \leftrightarrow u) \right\} + (1 \leftrightarrow 2) \right\} . \tag{B.41}
\end{aligned}$$

**Mixed chargino box involving vector Z coupling.** The generic form of these box diagrams is shown in Fig.1f,g, which are analogous to those in (d, e); but involve the vector  $Z\tilde{\chi}_1\tilde{\chi}_2$ -couplings in (A.5), combined with the  $g_{p12}^{h^0}$ ,  $g_{p12}^{H^0}$  Higgs ones of (A.10). The contribution of these diagrams may be obtained from those of Fig.1d,e by simply changing the sign of one chargino mass. More explicitly, if we write

$$F_{\lambda_1\lambda_2\lambda_Z}^{Z\nu\tilde{\chi}_1\tilde{\chi}_2\text{-box}}(\gamma\gamma \rightarrow Zh^0(H^0)) = r_{Z\nu\chi_1\chi_2}^{h^0(H^0)} \cdot A_{\lambda_1\lambda_2\lambda_Z}^{Z\nu\tilde{\chi}_1\tilde{\chi}_2\text{-box}}(H) , \tag{B.42}$$

where the relevant couplings defined in (A.5, A.10), are absorbed in the coefficients

$$\begin{aligned}
r_{Z\nu\chi_1\chi_2}^{h^0} &= -\frac{e^3}{(4\pi)^2} g_{v12}^Z g_{p12}^{h^0} , \\
r_{Z\nu\chi_1\chi_2}^{H^0} &= -\frac{e^3}{(4\pi)^2} g_{v12}^Z g_{p12}^{H^0} , \tag{B.43}
\end{aligned}$$

and the amplitudes  $A_{\lambda_1\lambda_2\lambda_Z}^{Z\nu\tilde{\chi}_1\tilde{\chi}_2\text{-box}}$  of (B.42) are determined by (B.38-B.41) through

$$A_{\lambda_1\lambda_2\lambda_Z}^{Z\nu\tilde{\chi}_1\tilde{\chi}_2\text{-box}}(H, m_{\tilde{\chi}_1}, m_{\tilde{\chi}_2}) = A_{\lambda_1\lambda_2\lambda_Z}^{Z\nu\tilde{\chi}_1\tilde{\chi}_2\text{-box}}(H, m_{\tilde{\chi}_1}, -m_{\tilde{\chi}_2}) = -A_{\lambda_1\lambda_2\lambda_Z}^{Z\nu\tilde{\chi}_1\tilde{\chi}_2\text{-box}}(H, -m_{\tilde{\chi}_1}, m_{\tilde{\chi}_2}) . \tag{B.44}$$

Notice that the constraint on  $A_{\lambda_1\lambda_2\lambda_Z}^{Z\nu\tilde{\chi}_1\tilde{\chi}_2\text{-box}}(H, m_{\tilde{\chi}_1}, m_{\tilde{\chi}_2})$  implied by (B.44), is satisfied by the expressions in (B.38-B.41).

Concerning the SM case  $\gamma\gamma \rightarrow ZH_{SM}$ , we note that it can be obtained from (B.26, B.29), by replacing  $h^0 \rightarrow H_{SM}$  and using  $\alpha = \beta - \pi/2$ .

## Appendix C: The $\gamma\gamma \rightarrow ZA^0$ helicity amplitudes.

The helicity amplitudes for  $\gamma\gamma \rightarrow ZA^0$

$$\gamma(k_1, \lambda_1)\gamma(k_2, \lambda_2) \rightarrow Z(q_1, \lambda_Z) A^0(q_2) \quad , \quad (\text{C.1})$$

denoted again as  $F_{\lambda_1\lambda_2\lambda_Z}(\kappa, t, u)$ , should satisfy the constraints

$$F_{\lambda_1, \lambda_2, \lambda_Z}(\kappa, t, u) = F_{-\lambda_1, -\lambda_2, -\lambda_Z}(\kappa, t, u)(-1)^{\lambda_Z} \quad , \quad (\text{C.2})$$

$$F_{\lambda_1\lambda_2\lambda_Z}(\kappa, t, u) = F_{\lambda_2\lambda_1\lambda_Z}(\kappa, u, t)(-1)^{\lambda_Z} \quad , \quad (\text{C.3})$$

$$F_{\lambda_1, \lambda_2, \lambda_Z}(\kappa, t, u) = -F_{\lambda_1, \lambda_2, -\lambda_Z}(-\kappa, t, u)(-1)^{\lambda_Z} \quad , \quad (\text{C.4})$$

imposed respectively by CP-invariance at the 1-loop level, Bose statistics and the structure of the Z-polarization vector. Thus, for the  $A^0$  production case also, there are only four "basic" helicity amplitudes which are taken as

$$F_{+++} \quad , \quad F_{+--} \quad , \quad F_{++0} \quad , \quad F_{+-0} \quad . \quad (\text{C.5})$$

Because of (C.2-C.4), the  $A^0$  production amplitudes still obey (B.8, B.9), but (B.10) is modified to

$$\begin{aligned} F_{+-0}(\kappa, t, u) &= -F_{+-0}(-\kappa, t, u) = F_{-+0}(\kappa, t, u) \\ &= F_{+-0}(\kappa, u, t) = F_{-+0}(\kappa, u, t) \quad . \end{aligned} \quad (\text{C.6})$$

The relevant diagrams are shown in Fig.2. Below we discuss their respective contributions.

**The  $h^0$ ,  $H^0$  pole contribution.** This is described by the diagram in Fig.2a, where the blob denotes loops from fermions, W-bosons and scalars.

As in (B.24), the only non-vanishing contribution from this diagram is for the  $F_{++0}$  amplitude. The fermion loop contributions to it is

$$\begin{aligned} F_{++0}^{(h^0, H^0)f\text{-pole}}(\gamma\gamma \rightarrow ZA^0) &= -\frac{i\alpha g\kappa m_f Q_f^2 N_f^c}{2c_W m_Z \pi} [(s - 4m_f^2)C_0^f(s) - 2] \left[ \frac{g_{h^0 ff} \cos(\beta - \alpha)}{s - m_{h^0}^2} \right. \\ &\quad \left. - \frac{g_{H^0 ff} \sin(\beta - \alpha)}{s - m_{H^0}^2 + im_{H^0}\Gamma_{H^0}} \right] \quad , \end{aligned} \quad (\text{C.7})$$

where the values of the  $g_{h^0 ff}$ ,  $g_{H^0 ff}$  couplings for the 3rd family fermions ( $t$ ,  $b$ ,  $\tau$ ) are given in (A.7). The same relation (C.7) describes also the chargino loop contribution to the  $\gamma\gamma h^0(H^0)$  vertex, provided  $(g_{h^0 ff}, g_{H^0 ff}) \rightarrow (g_j^{h^0}, g_j^{H^0})$ , with the later couplings given in (A.8, A.9).

For the  $W$  (plus Goldstone and ghost) contribution to the blob in Fig.2a, we have

$$\begin{aligned} F_{++0}^{(h^0, H^0)W\text{-pole}}(\gamma\gamma \rightarrow ZA^0) &= \\ &\frac{i\alpha^2 \kappa}{2s_W^2} \left\{ \left( \frac{1}{s - m_{h^0}^2} - \frac{1}{s - m_{H^0}^2} \right) [3 - (4s - 6m_W^2)C_0^W(s)] \sin 2(\beta - \alpha) \right. \\ &\quad \left. - \frac{\cos(2\beta)}{c_W^2} [1 + 2m_W^2 C_0^W(s)] \left[ \frac{\cos(\beta - \alpha) \sin(\beta + \alpha)}{s - m_{h^0}^2} + \frac{\sin(\beta - \alpha) \cos(\beta + \alpha)}{s - m_{H^0}^2} \right] \right\} \quad (\text{C.8}) \end{aligned}$$

Finally, the scalar contribution in the  $\gamma\gamma h^0(H^0)$  vertices give

$$F_{++0}^{(h^0, H^0)\text{scalar-pole}}(\gamma\gamma \rightarrow ZA^0) = \frac{i\alpha^2\kappa}{4s_W^2 m_W^2} \mathcal{H}^{\text{scalar}}(s), \quad (\text{C.9})$$

where for the charged Higgs loop we have

$$\begin{aligned} \mathcal{H}^{H^+}(s) &= 4m_W^2 \left[ 1 + 2m_{H^+}^2 C_0^{H^+}(s) \right] \left\{ \frac{\cos(\beta - \alpha)}{s - m_{h^0}^2} \left[ \sin(\beta - \alpha) + \frac{\cos(2\beta) \sin(\alpha + \beta)}{2c_W^2} \right] \right. \\ &\quad \left. - \frac{\sin(\beta - \alpha)}{s - m_{H^0}^2} \left[ \cos(\beta - \alpha) - \frac{\cos(2\beta) \cos(\alpha + \beta)}{2c_W^2} \right] \right\}, \end{aligned} \quad (\text{C.10})$$

for the lighter stop  $\tilde{t}_1$  loop

$$\begin{aligned} \mathcal{H}^{\tilde{t}_1}(s) &= 4 \left[ 1 + 2m_{\tilde{t}_1}^2 C_0^{\tilde{t}_1}(s) \right] \left\{ \frac{\cos(\beta - \alpha)}{s - m_{h^0}^2} \left[ -\frac{m_W^2}{c_W^2} \sin(\alpha + \beta) \left[ \frac{2s_W^2}{3} + \left( \frac{1}{2} - \frac{4s_W^2}{3} \right) \cos^2 \theta_t \right] \right. \right. \\ &\quad \left. \left. + \frac{m_t^2 \cos \alpha}{\sin \beta} + \frac{m_t(A_t \cos \alpha + \mu \sin \alpha)}{2 \sin \beta} \sin(2\theta_t) \text{Sign}(A_t - \mu \cot \beta) \right] \right. \\ &\quad \left. - \frac{\sin(\beta - \alpha)}{s - m_{H^0}^2} \left[ \frac{m_W^2}{c_W^2} \cos(\alpha + \beta) \left[ \frac{2s_W^2}{3} + \left( \frac{1}{2} - \frac{4s_W^2}{3} \right) \cos^2 \theta_t \right] + \frac{m_t^2 \sin \alpha}{\sin \beta} \right. \right. \\ &\quad \left. \left. + \frac{m_t(A_t \sin \alpha - \mu \cos \alpha)}{2 \sin \beta} \sin(2\theta_t) \text{Sign}(A_t - \mu \cot \beta) \right] \right\}, \end{aligned} \quad (\text{C.11})$$

while for the  $\tilde{t}_2$ -loop contribution we get

$$\begin{aligned} \mathcal{H}^{\tilde{t}_2}(s) &= 4 \left[ 1 + 2m_{\tilde{t}_2}^2 C_0^{\tilde{t}_2}(s) \right] \left\{ \frac{\cos(\beta - \alpha)}{s - m_{h^0}^2} \left[ -\frac{m_W^2}{c_W^2} \sin(\alpha + \beta) \left[ \frac{2s_W^2}{3} + \left( \frac{1}{2} - \frac{4s_W^2}{3} \right) \sin^2 \theta_t \right] \right. \right. \\ &\quad \left. \left. + \frac{m_t^2 \cos \alpha}{\sin \beta} - \frac{m_t(A_t \cos \alpha + \mu \sin \alpha)}{2 \sin \beta} \sin(2\theta_t) \text{Sign}(A_t - \mu \cot \beta) \right] \right. \\ &\quad \left. - \frac{\sin(\beta - \alpha)}{s - m_{H^0}^2} \left[ \frac{m_W^2}{c_W^2} \cos(\alpha + \beta) \left[ \frac{2s_W^2}{3} + \left( \frac{1}{2} - \frac{4s_W^2}{3} \right) \sin^2 \theta_t \right] + \frac{m_t^2 \sin \alpha}{\sin \beta} \right. \right. \\ &\quad \left. \left. - \frac{m_t(A_t \sin \alpha - \mu \cos \alpha)}{2 \sin \beta} \sin(2\theta_t) \text{Sign}(A_t - \mu \cot \beta) \right] \right\}, \end{aligned} \quad (\text{C.12})$$

where the various stop-parameters are defined as in [11].

**Singe fermion box contribution.** It is given by the diagram in Fig.2b which is closely related to the diagram in Fig.1c for the  $h^0, H^0$  production case. In both cases, the Z-coupling to fermions is axial, while the main difference stems from the  $\gamma_5$  in the Higgs vertex of Fig.2b. In analogy to (B.29), the contribution of the diagram in Fig.2b may be written as

$$F_{\lambda_1 \lambda_2 \lambda_Z}^{f\text{-box}}(\gamma\gamma \rightarrow ZA^0) = r_f^{A^0} \cdot A_{\lambda_1 \lambda_2 \lambda_Z}^{f\text{-box}}(A^0), \quad (\text{C.13})$$

with

$$\begin{aligned}
r_f^{A^0} &= i \frac{e^3}{(4\pi)^2} N_f^c Q_f^2 g_{af}^Z \tilde{g}^{A^0 ff} , \\
r_{\tilde{\chi}_j}^{A^0} &= i \frac{e^3}{(4\pi)^2} g_{aj}^Z \tilde{g}_j^{A^0}
\end{aligned} \tag{C.14}$$

for  $(t, b, \tau)$  and charginos respectively; (j=1,2 counts the two different charginos). The relevant  $(Z, A^0)$ -couplings appear in (A.2, A.7) and (A.3, A.4, A.8, A.9). For the amplitudes defined in (C.13) we find

$$A_{+++}^{f\text{-box}}(A^0) = -A_{+++}^{f\text{-box}}(H) , \tag{C.15}$$

$$A_{++0}^{f\text{-box}}(A^0) = -A_{++0}^{f\text{-box}}(H) , \tag{C.16}$$

where (B.32, B.34) should be used accompanied with the obvious replacement  $m \Rightarrow m_{A^0}$ . For the rest of the "basic" amplitudes in (C.5) we get

$$\begin{aligned}
A_{+--}^{f\text{-box}}(A^0) &= \frac{\sqrt{2}m_f}{\kappa\sqrt{Y}s} \left\{ (t_Z + u_Z)(\kappa + u - t) Y D_{hZ}^f(t, u) \right. \\
&+ (t_h + u_h)(\kappa + u - t) [2sC_0^f(s) - suD_{hZ}^f(s, u) - stD_{hZ}^f(s, t)] \\
&- 2[t_h(t - \kappa) + u_Z m^2 + Y][u_h C_h^f(u) + t_Z C_Z^f(t)] \\
&\left. + 2[u_h(u + \kappa) + t_Z m^2 + Y][u_Z C_Z^f(u) + t_h C_h^f(t)] \right\} ,
\end{aligned} \tag{C.17}$$

$$\begin{aligned}
A_{+-0}^{f\text{-box}}(A^0) &= \frac{4m_f}{\kappa m_Z Y} \left\{ (t^2 + u^2 - 2m^2 m_Z^2) [s(t + u)C_0^f(s) - \kappa^2 C_{hZ}^f(s)] \right. \\
&- 2m_f^2 \kappa^2 Y \tilde{F}^f(s, t, u) + 2m_Z^2 Y^2 D_{hZ}^f(t, u) + [u^2(t + u) - m^2 m_Z^2 (3u - t)] E_1^f(s, u) \\
&\left. + [t^2(t + u) - m^2 m_Z^2 (3t - u)] E_1^f(s, t) \right\} .
\end{aligned} \tag{C.18}$$

**Mixed chargino box contribution.** This is determined by the diagrams in Fig.2c,d which involve vector mixed Z-coupling to the two charginos, and those of Fig.2e,f containing axial mixed Z-couplings; compare (A.5). Their complete contribution may be written as

$$\begin{aligned}
F_{\lambda_1 \lambda_2 \lambda_Z}^{\tilde{\chi}_1 \tilde{\chi}_2 \text{-box}}(\gamma\gamma \rightarrow ZA^0) &= -\frac{\alpha e}{4\pi} \left[ g_{v12}^Z g_{s12}^{A^0} A_{\lambda_1 \lambda_2 \lambda_Z}^{\tilde{\chi}_1 \tilde{\chi}_2 \text{-box}}(A^0, m_{\tilde{\chi}_1}, m_{\tilde{\chi}_2}) \right. \\
&\left. - g_{a12}^Z g_{p12}^{A^0} A_{\lambda_1 \lambda_2 \lambda_Z}^{\tilde{\chi}_1 \tilde{\chi}_2 \text{-box}}(A^0, m_{\tilde{\chi}_1}, -m_{\tilde{\chi}_2}) \right] ,
\end{aligned} \tag{C.19}$$

where the two terms in the r.h.s. arise from the diagrams in Fig.2(c,d) and (e,f) respectively; and the Z- and  $A^0$  couplings appear in (A.5, A.10). Thus only the (c,d) diagrams need to be calculated.

Defining also

$$\begin{aligned} Q_A &= -4s(m_{\tilde{\chi}_1}^2 + m_{\tilde{\chi}_2}^2) + 4u_h u_Z + s^2 + m^2 s - m_Z^2 s + 4su, \\ \bar{Q}_A &= -\kappa^2(m^2 + m_Z^2) + (t+u)(t-u)^2 + 8m_Z^2 Y, \end{aligned} \quad (\text{C.20})$$

$$\begin{aligned} P_{tu}^+ &= 2(t-u)Y \left\{ -2s(m_{\tilde{\chi}_1}^2 + m_{\tilde{\chi}_2}^2)(m_{\tilde{\chi}_1} + m_{\tilde{\chi}_2})^2 - (m_{\tilde{\chi}_1} + m_{\tilde{\chi}_2})^2 [2Y - s(t_Z + u_Z)] \right. \\ &\quad \left. + Y(t_Z + u_Z) \right\}, \\ Q_{tu}^+ &= 4(m_{\tilde{\chi}_1} + m_{\tilde{\chi}_2})^2 (t-u) \left\{ 2s^2(m_{\tilde{\chi}_1}^2 - m_{\tilde{\chi}_2}^2)^2 + 3s(m_{\tilde{\chi}_1}^2 + m_{\tilde{\chi}_2}^2)Y + Y^2 \right\}, \\ P_{tu}^- &= 2 \left\{ 2s(t_Z + u_Z)(m_{\tilde{\chi}_1}^2 - m_{\tilde{\chi}_2}^2)^2 - (m_{\tilde{\chi}_1} - m_{\tilde{\chi}_2})^2 s(t^2 + u^2 - 2m^2 m_Z^2) \right. \\ &\quad \left. + 2(m_{\tilde{\chi}_1}^2 + m_{\tilde{\chi}_2}^2)Y(t_Z + u_Z) - Y(t^2 + u^2 - 2m^2 m_Z^2) \right\}, \\ Q_{tu}^- &= 4 \left\{ s(t_Z + u_Z)(m_{\tilde{\chi}_1}^2 - m_{\tilde{\chi}_2}^2)^2 + (m_{\tilde{\chi}_1}^2 + m_{\tilde{\chi}_2}^2)Y(m^2 - m_Z^2 - 2s) \right. \\ &\quad \left. + 2m_{\tilde{\chi}_1} m_{\tilde{\chi}_2} sY - Y^2 \right\}, \end{aligned} \quad (\text{C.21})$$

$$\begin{aligned} P_{su}^+ &= 2Y \left\{ -2(t-u)(m_{\tilde{\chi}_1} + m_{\tilde{\chi}_2})^2 (m_{\tilde{\chi}_1}^2 + m_{\tilde{\chi}_2}^2) \right. \\ &\quad \left. + (m_{\tilde{\chi}_1} + m_{\tilde{\chi}_2})^2 (2uu_h + 6u_h u_Z + \kappa^2 - 2m_Z^2 t_h) - u(t-u)(t_h + u_h) \right\}, \\ Q_{su}^+ &= 4(m_{\tilde{\chi}_1} + m_{\tilde{\chi}_2})^2 \left\{ 2s(t-u)(m_{\tilde{\chi}_1}^2 - m_{\tilde{\chi}_2}^2)^2 + 3(t-u)Y(m_{\tilde{\chi}_1}^2 + m_{\tilde{\chi}_2}^2) \right. \\ &\quad \left. + (Y + 2u_Z u_h)[3(u^2 - m^2 m_Z^2) - Y] \right\}, \\ P_{su}^- &= -2Y \left\{ -2(2s+t-u)(m_{\tilde{\chi}_1}^2 - m_{\tilde{\chi}_2}^2)^2 - (t-u)(t_h + u_h)(m_{\tilde{\chi}_1} - m_{\tilde{\chi}_2})^2 \right. \\ &\quad \left. + 2(m_{\tilde{\chi}_1}^2 + m_{\tilde{\chi}_2}^2)(u^2 - m^2 m_Z^2 - 3Y) + u[4ut_h + t^2 + 3u^2 - 2m_Z^2(t+u)] \right\}, \\ Q_{su}^- &= -4 \left\{ (m_{\tilde{\chi}_1}^2 - m_{\tilde{\chi}_2}^2)^2 \left[ (m^2 + m_Z^2)[4Y - 6(u^2 - m^2 m_Z^2)] + 6u^3 - tu(t+u) \right] \right. \\ &\quad \left. + m^2 m_Z^2 (u - 5t) \right\} + Y[Y - 3(u^2 - m^2 m_Z^2)](m_{\tilde{\chi}_1}^2 + m_{\tilde{\chi}_2}^2) \\ &\quad - 2su^2(u^2 - m^2 m_Z^2) \left. \right\}. \end{aligned} \quad (\text{C.22})$$

we find for the basic amplitudes (compare (C.5))

$$\begin{aligned} &A_{++++}^{\tilde{\chi}_1 \tilde{\chi}_2 - \text{box}}(A^0, m_{\tilde{\chi}_1}, m_{\tilde{\chi}_2}) = \\ &\frac{\sqrt{2}}{8\kappa\sqrt{s^3 Y}} \left\{ \left[ -8s^2(t-u)m_{\tilde{\chi}_1}[t_h + u_h - \kappa + 4m_{\tilde{\chi}_1}(m_{\tilde{\chi}_1} + m_{\tilde{\chi}_2})]C_0^{111}(s) \right. \right. \\ &\quad \left. \left. + 4s(m_{\tilde{\chi}_1} - m_{\tilde{\chi}_2})u_h \left\{ (\kappa + u - t)[2(m_{\tilde{\chi}_1} + m_{\tilde{\chi}_2})^2 + t_h] - 2Y \right\} [C_h^{211}(u) + C_h^{122}(u)] \right. \right. \\ &\quad \left. \left. - 8(m_{\tilde{\chi}_1} + m_{\tilde{\chi}_2})Y(\kappa - t_Z - u_Z) \left\{ u_h [C_h^{211}(u) - C_h^{122}(u)] - u_Z [C_Z^{211}(u) - C_Z^{122}(u)] \right\} \right] \right\} \end{aligned}$$

$$\begin{aligned}
& -4s(m_{\tilde{\chi}_1} - m_{\tilde{\chi}_2})u_Z \left\{ (\kappa + t - u)[2(m_{\tilde{\chi}_1} + m_{\tilde{\chi}_2})^2 + u_h] - 2Y \right\} [C_Z^{211}(u) + C_Z^{122}(u)] \\
& -8s^2 m_{\tilde{\chi}_1} [4m_{\tilde{\chi}_1}(m_{\tilde{\chi}_1} + m_{\tilde{\chi}_2}) + t_h + u_h - \kappa] [Y + u^2 - m^2 m_Z^2 \\
& - (t - u)(m_{\tilde{\chi}_1}^2 - m_{\tilde{\chi}_2}^2)] D_{hZ}^{1211}(s, u) - s(m_{\tilde{\chi}_1} - m_{\tilde{\chi}_2})(t - u) \left\{ \kappa[s(m_{\tilde{\chi}_1} + m_{\tilde{\chi}_2})^2 + Y] \right. \\
& - (t_h + u_h)Y + (m_{\tilde{\chi}_1} + m_{\tilde{\chi}_2})^2 Q_A \left. \right\} [D_{hZ}^{1221}(t, u) + D_{hZ}^{2112}(t, u)] + (m_{\tilde{\chi}_1} + m_{\tilde{\chi}_2}) \left\{ Y \bar{Q}_A \right. \\
& - \kappa[s(m_{\tilde{\chi}_1} - m_{\tilde{\chi}_2})^2 + Y](Q_A - 8m_{\tilde{\chi}_1} m_{\tilde{\chi}_2} s) + s[\bar{Q}_A(m_{\tilde{\chi}_1}^2 + m_{\tilde{\chi}_2}^2) \\
& \left. + 2m_{\tilde{\chi}_1} m_{\tilde{\chi}_2} s \kappa^2] \right\} [D_{hZ}^{1221}(t, u) - D_{hZ}^{2112}(t, u)] - (t \leftrightarrow u) - (1 \leftrightarrow 2) \left. \right\}, \tag{C.23}
\end{aligned}$$

$$\begin{aligned}
& A_{+--}^{\tilde{\chi}_1 \tilde{\chi}_2 \text{-box}}(A^0, m_{\tilde{\chi}_1}, m_{\tilde{\chi}_2}) = \\
& \frac{1}{\kappa \sqrt{2sY^3}} \left\{ 8(m_{\tilde{\chi}_1} + m_{\tilde{\chi}_2})sY(\kappa + t - u)[B_0(s, m_{\tilde{\chi}_1}, m_{\tilde{\chi}_1}) - B_0(s, m_{\tilde{\chi}_2}, m_{\tilde{\chi}_2})] \right. \\
& - 2(m_{\tilde{\chi}_1} - m_{\tilde{\chi}_2})s \left\{ (t - u - \kappa)Y[t_h + u_h + 2(m_{\tilde{\chi}_1} + m_{\tilde{\chi}_2})^2] \right. \\
& \left. + 2(u - t - \kappa)(m_{\tilde{\chi}_1} + m_{\tilde{\chi}_2})^2[Y + 2s(t + u)] \right\} [C_0^{111}(s) + C_0^{222}(s)] \\
& + 2(m_{\tilde{\chi}_1} + m_{\tilde{\chi}_2})s \left\{ (u - t + \kappa)Y[t_h + u_h + 2(m_{\tilde{\chi}_1}^2 + m_{\tilde{\chi}_2}^2)] + 2(t - u + \kappa)[Y(m_{\tilde{\chi}_1}^2 + m_{\tilde{\chi}_2}^2) \right. \\
& \left. + 2s(m_{\tilde{\chi}_1}^2 - m_{\tilde{\chi}_2}^2)^2 + s(t^2 - m^2 m_Z^2) + su(t + u)] \right\} [C_0^{111}(s) - C_0^{222}(s)] \\
& - 8(m_{\tilde{\chi}_1} - m_{\tilde{\chi}_2})(m_{\tilde{\chi}_1} + m_{\tilde{\chi}_2})^2 s \kappa \left\{ \kappa(t - u) + t^2 + u^2 - 2m^2 m_Z^2 \right\} [C_{hZ}^{121}(s) + C_{hZ}^{212}(s)] \\
& - 4(m_{\tilde{\chi}_1} + m_{\tilde{\chi}_2})s(t + u)\kappa \left\{ \kappa(t - u) + t^2 + u^2 - 2m^2 m_Z^2 \right\} [C_{hZ}^{121}(s) - C_{hZ}^{212}(s)] \\
& - \frac{(m_{\tilde{\chi}_1} - m_{\tilde{\chi}_2})}{2(u - t)} \left\{ P_{tu}^+(\kappa + u - t) + Q_{tu}^+(-\kappa + u - t) \right\} [D_{hZ}^{1221}(t, u) + D_{hZ}^{2112}(t, u)] \\
& + \frac{(m_{\tilde{\chi}_1} + m_{\tilde{\chi}_2})}{2(u - t)} Y \left\{ P_{tu}^-(\kappa + u - t) + Q_{tu}^-(-\kappa + u - t) \right\} [D_{hZ}^{1221}(t, u) - D_{hZ}^{2112}(t, u)] \\
& + \left[ 2(m_{\tilde{\chi}_1} - m_{\tilde{\chi}_2})u_h \left\{ 2(m_{\tilde{\chi}_1} + m_{\tilde{\chi}_2})^2[-2m^2(u^2 - m^2 m_Z^2) - 4m_Z^2 Y + 3(t + u)Y \right. \right. \\
& \left. \left. + 2u(uu_Z - tt_Z)] - Y(Y + m^2 u_Z + tt_h) \right. \right. \\
& \left. \left. + \kappa[-2(m_{\tilde{\chi}_1} + m_{\tilde{\chi}_2})^2(Y + 2u_Z u_h) + t_h Y] \right\} [C_h^{211}(u) + C_h^{122}(u)] \right. \\
& \left. + 2(m_{\tilde{\chi}_1} - m_{\tilde{\chi}_2})u_Z \left\{ 2(m_{\tilde{\chi}_1} + m_{\tilde{\chi}_2})^2[(2u_h + t)(u^2 - m^2 m_Z^2) - 2m_Z^2 u(u - t) - u(t^2 - m^2 m_Z^2)] \right. \right. \\
& \left. \left. + Y(Y + m^2 t_Z + uu_h) + \kappa[-2(m_{\tilde{\chi}_1} + m_{\tilde{\chi}_2})^2(Y + 2u_Z u_h) + u_h Y] \right\} [C_Z^{211}(u) + C_Z^{122}(u)] \right. \\
& \left. - 4(m_{\tilde{\chi}_1} + m_{\tilde{\chi}_2})su(Y + u^2 - m^2 m_Z^2 - \kappa u) \left\{ u_h[C_h^{211}(u) - C_h^{122}(u)] + u_Z[C_Z^{211}(u) - C_Z^{122}(u)] \right\} \right. \\
& \left. - \frac{(m_{\tilde{\chi}_1} - m_{\tilde{\chi}_2})s}{2(u - t)} \left\{ P_{su}^+(\kappa + u - t) + Q_{su}^+(-\kappa + u - t) \right\} [D_{hZ}^{1211}(s, u) + D_{hZ}^{2122}(s, u)] \right. \\
& \left. + \frac{(m_{\tilde{\chi}_1} + m_{\tilde{\chi}_2})s}{2(u - t)} \left\{ P_{su}^-(\kappa + u - t) + Q_{su}^-(-\kappa + u - t) \right\} [D_{hZ}^{1211}(s, u) - D_{hZ}^{2122}(s, u)] \right.
\end{aligned}$$

$$- (t \leftrightarrow u, \kappa \rightarrow -\kappa) \Big] \Big\} , \quad (\text{C.24})$$

$$\begin{aligned}
& A_{++0}^{\tilde{\chi}_1 \tilde{\chi}_2 - \text{box}}(A^0, m_{\tilde{\chi}_1}, m_{\tilde{\chi}_2}) = \\
& \frac{1}{2\kappa m_Z s} \left\{ 8(m_{\tilde{\chi}_1} - m_{\tilde{\chi}_2})s[s(t+u) - 2(m_{\tilde{\chi}_1} + m_{\tilde{\chi}_2})^2(t_Z + u_Z)][C_0^{111}(s) + C_0^{222}(s)] \right. \\
& + 8(m_{\tilde{\chi}_1} + m_{\tilde{\chi}_2})s[s(t+u) - 2(m_{\tilde{\chi}_1}^2 + m_{\tilde{\chi}_2}^2)(t_Z + u_Z)][C_0^{111}(s) - C_0^{222}(s)] \\
& - 4(m_{\tilde{\chi}_1} - m_{\tilde{\chi}_2}) \left\{ Y[(t+u)(m^2 + m_Z^2) - 4m^2 m_Z^2] - 2s(t_Z + u_Z)(m_{\tilde{\chi}_1}^2 + m_{\tilde{\chi}_2}^2)(m_{\tilde{\chi}_1} + m_{\tilde{\chi}_2})^2 \right. \\
& \left. + \frac{(m_{\tilde{\chi}_1} + m_{\tilde{\chi}_2})^2}{2}(t_Z + u_Z)(4u_Z u_h + sm^2 + ss_Z + 4su) + \frac{(m_{\tilde{\chi}_1} - m_{\tilde{\chi}_2})^2}{2}s\kappa^2 \right\} \cdot \\
& \cdot [D_{hZ}^{1221}(t, u) + D_{hZ}^{2112}(t, u)] \\
& + 8(m_{\tilde{\chi}_1} + m_{\tilde{\chi}_2})m_Z^2(t-u)[s(m_{\tilde{\chi}_1}^2 + m_{\tilde{\chi}_2}^2) + Y][D_{hZ}^{1221}(t, u) - D_{hZ}^{2112}(t, u)] \\
& + \left[ 4(m_{\tilde{\chi}_1} - m_{\tilde{\chi}_2})[(t+u)(m^2 + m_Z^2) - 4m^2 m_Z^2 - 2(m_{\tilde{\chi}_1} + m_{\tilde{\chi}_2})^2(t_Z + u_Z)] \cdot \right. \\
& \left. \cdot \left\{ u_h[C_h^{211}(u) + C_h^{122}(u)] + u_Z[C_Z^{211}(u) + C_Z^{122}(u)] \right\} \right. \\
& + 8(m_{\tilde{\chi}_1} + m_{\tilde{\chi}_2})m_Z^2(u-t) \left\{ u_h[C_h^{211}(u) - C_h^{122}(u)] - u_Z[C_Z^{211}(u) - C_Z^{122}(u)] \right\} \\
& + 4(m_{\tilde{\chi}_1} - m_{\tilde{\chi}_2})s \left\{ 2(t_Z + u_Z)(m_{\tilde{\chi}_1}^2 + m_{\tilde{\chi}_2}^2)(m_{\tilde{\chi}_1} + m_{\tilde{\chi}_2})^2 - 2sm^2 m_Z^2 \right. \\
& \left. + (m_{\tilde{\chi}_1}^2 + m_{\tilde{\chi}_2}^2)[8m^2 m_Z^2 - (t+u)(m^2 + 3m_Z^2)] + 2m_{\tilde{\chi}_1} m_{\tilde{\chi}_2} [s^2 + (m_Z^2 - m^2)(s - 2m_Z^2)] \right\} \cdot \\
& \cdot [D_{hZ}^{1211}(s, u) + D_{hZ}^{2122}(s, u)] \\
& + 4(m_{\tilde{\chi}_1} + m_{\tilde{\chi}_2})s \left\{ 2(t_Z + u_Z)(m_{\tilde{\chi}_1}^2 - m_{\tilde{\chi}_2}^2)^2 - 2sm^2 m_Z^2 + (m_{\tilde{\chi}_1}^2 + m_{\tilde{\chi}_2}^2)[8m^2 m_Z^2 \right. \\
& \left. - (t+u)(m^2 + 3m_Z^2)] - 2m_{\tilde{\chi}_1} m_{\tilde{\chi}_2} [4m^2 m_Z^2 - (t+u)(m^2 + m_Z^2)] \right\} [D_{hZ}^{1211}(s, u) - D_{hZ}^{2122}(s, u)] \\
& \left. + (u \leftrightarrow t) \right\} , \quad (\text{C.25})
\end{aligned}$$

$$\begin{aligned}
& A_{+-0}^{\tilde{\chi}_1 \tilde{\chi}_2 - \text{box}}(A^0, m_{\tilde{\chi}_1}, m_{\tilde{\chi}_2}) = \frac{1}{\kappa m_Z Y} \left\{ - (m_{\tilde{\chi}_1} - m_{\tilde{\chi}_2})s \left\{ 2(m_{\tilde{\chi}_1} + m_{\tilde{\chi}_2})^2[\kappa^2 - 4m_Z^2(t_h + u_h)] \right. \right. \\
& \left. \left. - (t+u)(t^2 + u^2 - 2m^2 m_Z^2) \right\} [C_0^{111}(s) + C_0^{222}(s)] + 2(m_{\tilde{\chi}_1} + m_{\tilde{\chi}_2})s \left\{ (m_{\tilde{\chi}_1} - m_{\tilde{\chi}_2})^2 \kappa^2 \right. \right. \\
& \left. \left. - 2(t_Z + u_Z)(m_{\tilde{\chi}_1}^2 - m_{\tilde{\chi}_2}^2)^2 + m_Z^2(2m^2 s_h + t^2 + u^2) \right\} [C_0^{111}(s) - C_0^{222}(s)] \right. \\
& + (m_{\tilde{\chi}_1} - m_{\tilde{\chi}_2}) \left\{ (t^2 + u^2 - 2m^2 m_Z^2)[2(t_Z + u_Z)(m_{\tilde{\chi}_1} + m_{\tilde{\chi}_2})^2 - \kappa^2] \right\} [C_{hZ}^{121}(s) + C_{hZ}^{212}(s)] \\
& - 2(m_{\tilde{\chi}_1} + m_{\tilde{\chi}_2})m_Z^2(t_h + u_h)(t^2 + u^2 - 2m^2 m_Z^2)[C_{hZ}^{121}(s) - C_{hZ}^{212}(s)] \\
& + 2(m_{\tilde{\chi}_1} - m_{\tilde{\chi}_2})u_h \left\{ u(u^2 - m^2 m_Z^2) + uY + m^2 m_Z^2(t-u) \right. \\
& \left. - 2(m_{\tilde{\chi}_1} + m_{\tilde{\chi}_2})^2(2m_Z^2 s_Z + u^2 + tu) \right\} [C_h^{211}(u) + C_h^{122}(u)] \\
& + 2(m_{\tilde{\chi}_1} - m_{\tilde{\chi}_2})u_Z \left\{ u(u^2 - m^2 m_Z^2) + uY + m^2 m_Z^2(t-u) \right.
\end{aligned}$$



$$\begin{aligned}
& -2(m_{\tilde{\chi}_1} + m_{\tilde{\chi}_2})^2(2m_Z^2m_Z^2 - 4um_Z^2 + u^2 + tu) \Big\} [C_Z^{211}(u) + C_Z^{122}(u)] \\
& + 4(m_{\tilde{\chi}_1} + m_{\tilde{\chi}_2})m_Z^2u(t_h + u_h) \Big\{ u_h[C_h^{211}(u) - C_h^{122}(u)] + u_Z[C_Z^{211}(u) - C_Z^{122}(u)] \Big\} \\
& - 2(m_{\tilde{\chi}_1} - m_{\tilde{\chi}_2}) \Big\{ -2(t_Z + u_Z)(m_{\tilde{\chi}_1} + m_{\tilde{\chi}_2})^2[s(m_{\tilde{\chi}_1}^2 - m_{\tilde{\chi}_2}^2)^2 + Y(m_{\tilde{\chi}_1}^2 + m_{\tilde{\chi}_2}^2)] \\
& + s\kappa^2(m_{\tilde{\chi}_1}^2 - m_{\tilde{\chi}_2}^2)^2 + 2(m_{\tilde{\chi}_1} + m_{\tilde{\chi}_2})^2[u_h m_Z^6 + m_Z^4(m^4 - u^2 + 2m^2s - su) \\
& + uu_h m_Z^2(3s + m^2) + su^2 s_h] + su(u^3 + tu^2 - 3m_Z^2 m^2 u + m^2 m_Z^2 t) \\
& + \kappa^2 Y(m_{\tilde{\chi}_1}^2 + m_{\tilde{\chi}_2}^2) \Big\} [D_{hZ}^{1211}(s, u) + D_{hZ}^{2122}(s, u)] \\
& + 2(m_{\tilde{\chi}_1} + m_{\tilde{\chi}_2}) \Big\{ -2(m_{\tilde{\chi}_1}^2 - m_{\tilde{\chi}_2}^2)^2[m^2(u^2 - m_Z^4) - m^4 u_Z - 2m^2 m_Z^2 s - m_Z^2(s - u)^2 \\
& + su(s - u) + m_Z^4(s + u)] - (m_{\tilde{\chi}_1} - m_{\tilde{\chi}_2})^2\{2m_Z^2 m^2(2m_Z^2 m^2 - t^2 + 3u^2) \\
& + (m^2 + m_Z^2)[m^2 m_Z^2(t - 7u) + 2u^3 + 3tu^2 + t^2 u] - 2u^2(t + u)^2\} \\
& - 2m_Z^2 Y(m_{\tilde{\chi}_1}^2 + m_{\tilde{\chi}_2}^2)(t_h + u_h) - 2sum_Z^2(u^2 - m^2 m_Z^2 - 2m^2 u_Z) \Big\} [D_{hZ}^{1211}(s, u) - D_{hZ}^{2122}(s, u)] \\
& + 2(m_{\tilde{\chi}_1} + m_{\tilde{\chi}_2})m_Z^2(t - u)[s(m_{\tilde{\chi}_1}^2 - m_{\tilde{\chi}_2}^2)^2 + (m_{\tilde{\chi}_1}^2 + m_{\tilde{\chi}_2}^2)Y] [D_{hZ}^{1221}(t, u) - D_{hZ}^{2112}(t, u)] \\
& - (m_{\tilde{\chi}_1} - m_{\tilde{\chi}_2}) \Big\{ [(m_{\tilde{\chi}_1}^2 - m_{\tilde{\chi}_2}^2)^2 s + (m_{\tilde{\chi}_1}^2 + m_{\tilde{\chi}_2}^2)Y][\kappa^2 - 2(t_Z + u_Z)(m_{\tilde{\chi}_1} + m_{\tilde{\chi}_2})^2] \\
& - 2m_Z^2 Y[s(m_{\tilde{\chi}_1} + m_{\tilde{\chi}_2})^2 + Y] \Big\} [D_{hZ}^{1221}(t, u) + D_{hZ}^{2112}(t, u)] + (t \leftrightarrow u) \Big\} . \tag{C.26}
\end{aligned}$$

## References

- [1] For recent reviews see e.g., I.F. Ginzburg, hep-ph/0101029 and E.Boos et al, hep-ph/0103090.
- [2] I.F. Ginzburg, G.L. Kotkin, V.G. Serbo and V.I. Telnov, Nucl. Instr. and Meth. **205**, 47 (1983); I.F. Ginzburg, G.L. Kotkin, V.G. Serbo, S.L. Panfil and V.I. Telnov, Nucl. Instr. and Meth. **219**,5 (1984); J.H. Kühn, E.Mirkes and J. Steegborn, Z. f. Phys. **C57**, 615 (1993).
- [3] V. Telnov, hep-ex/0003024, hep-ex/0001029, hep-ex/9802003, hep-ex/9805002, hep-ex/9908005; I.F. Ginzburg, hep-ph/9907549; R. Brinkman hep-ex/9707017. V. Telnov, talk at the International Workshop on High Energy Photon Colliders, <http://www.desy.de/gg2000>, June 14-17, 2000, DESY Hamburg, Germany, to appear in Nucl.Instr. & Meth. A.; D.S. Gorbunov, V.A. Illyn, V.I. Telnov, hep-ph/0012175.
- [4] Opportunities and Requirements for Experimentation at a Very High Energy  $e^+e^-$  Collider, SLAC-329(1928); Proc. Workshops on Japan Linear Collider, KEK Reports, 90-2, 91-10 and 92-16; P.M. Zerwas, DESY 93-112, Aug. 1993; Proc. of the Workshop on  $e^+e^-$  Collisions at 500 GeV: The Physics Potential, DESY 92-123A,B,(1992), C(1993), D(1994), E(1997) ed. P. Zerwas; E. Accomando *et.al.* Phys. Rep. **C299**, 299 (1998).
- [5] " The CLIC study of a multi-TeV  $e^+e^-$  linear collider" , CERN-PS-99-005-LP (1999).
- [6] J.F. Gunion, H.E. Haber, G. Kane and S. Dawson, "The Higgs Hunter's Guide", Addison-Wesley, Redwood City (1990); D.L. Borden, D.A. Bauer and D.O. Caldwell, Phys. Rev. **D48**, 1993 (4018); G.J. Gounaris and G.P. Tsirigoti, hep-ph/9703446, Phys. Rev. **D56**, 3030 (1997), Phys. Rev. **D58**, 059901 (1998); M. Baillargeon, G. Belanger and F. Boudjema, hep-ph/9405359; J.F. Gunion, in Perspectives on Higgs Particles, hep-ph/9705282. A. Djouadi, V. Driesen, W. Hollik and J.I. Illana, Eur. Phys. J. **C1**, 163 (1998).
- [7] E.W.N. Glover and J.J. van der Bij, Nucl. Phys. **B321**, 561 (1989); G. Jikia Nucl. Phys. **B405**, 24 (1993); Phys. Lett. **B298**, 1993 (224); G. Jikia and A. Tkabladze, Phys. Lett. **B332**, 1994 (441); G. Jikia and A. Tkabladze, Phys. Lett. **B323**, 1994 (453); B. Bajc Phys. Rev. **D48**, 1993 (R1907); M.S. Berger Phys. Rev. **D48**, 1993 (5121); D.A. Dicus and C. Kao, Phys. Rev. **D49**, 1994 (1265); M.S. Berger, M.S. Chanowitz, Nucl.Instrum.Meth.,**A355**,52(1995).
- [8] G.J. Gounaris, P.I. Porfyriadis, F.M. Renard, hep-ph/9812378, Phys. Lett. **B452**, 76 (1999), Phys. Lett. **B464**, 350 (1999) (E); G.J. Gounaris, P.I. Porfyriadis, F.M. Renard, hep-ph/9902230, Eur. Phys. J. **C9**, 673 (1999).

- [9] G.J. Gounaris, J. Layssac, P.I. Porfyriadis and F.M. Renard, hep-ph/9904450, Eur. Phys. J. **C10**, 499 (1999).
- [10] G.J. Gounaris, J. Layssac, P.I. Porfyriadis and F.M. Renard, hep-ph/9909243, Eur. Phys. J. **C13**, 79 (2000).
- [11] G.J. Gounaris, J. Layssac, P.I. Porfyriadis and F.M. Renard, hep-ph/0010006, to appear in Eur. Phys. Journal C.
- [12] A. Djouadi, J. Kalinowski and M. Spira, HDECAY, hep-ph/9704448, Comput. Phys. Commun. **108**, 56 (1998).
- [13] A. Djouadi, J.L. Kneur and G. Moultaka, Nucl. Phys. **B560**, 53 (2000); C. Le Mouél, hep-ph/0101351.
- [14] M.M. Mühlleitner, Dissertation at the University of Hamburg, hep-ph/0008127; H. E. Haber *et.al.* hep-ph/0007006.
- [15] G. Passarino and M. Veltman, Nucl. Phys. **B160**, 151 (1979).
- [16] K. Hagiwara, S. Matsumoto, D. Haidt and C.S. Kim, Z. f. Phys. **C64**, 559 (1995).
- [17] G.J. Gounaris and P.I. Porfyriadis, hep-ph/0007110, Eur. Phys. J. **C18**, 181 (2000).

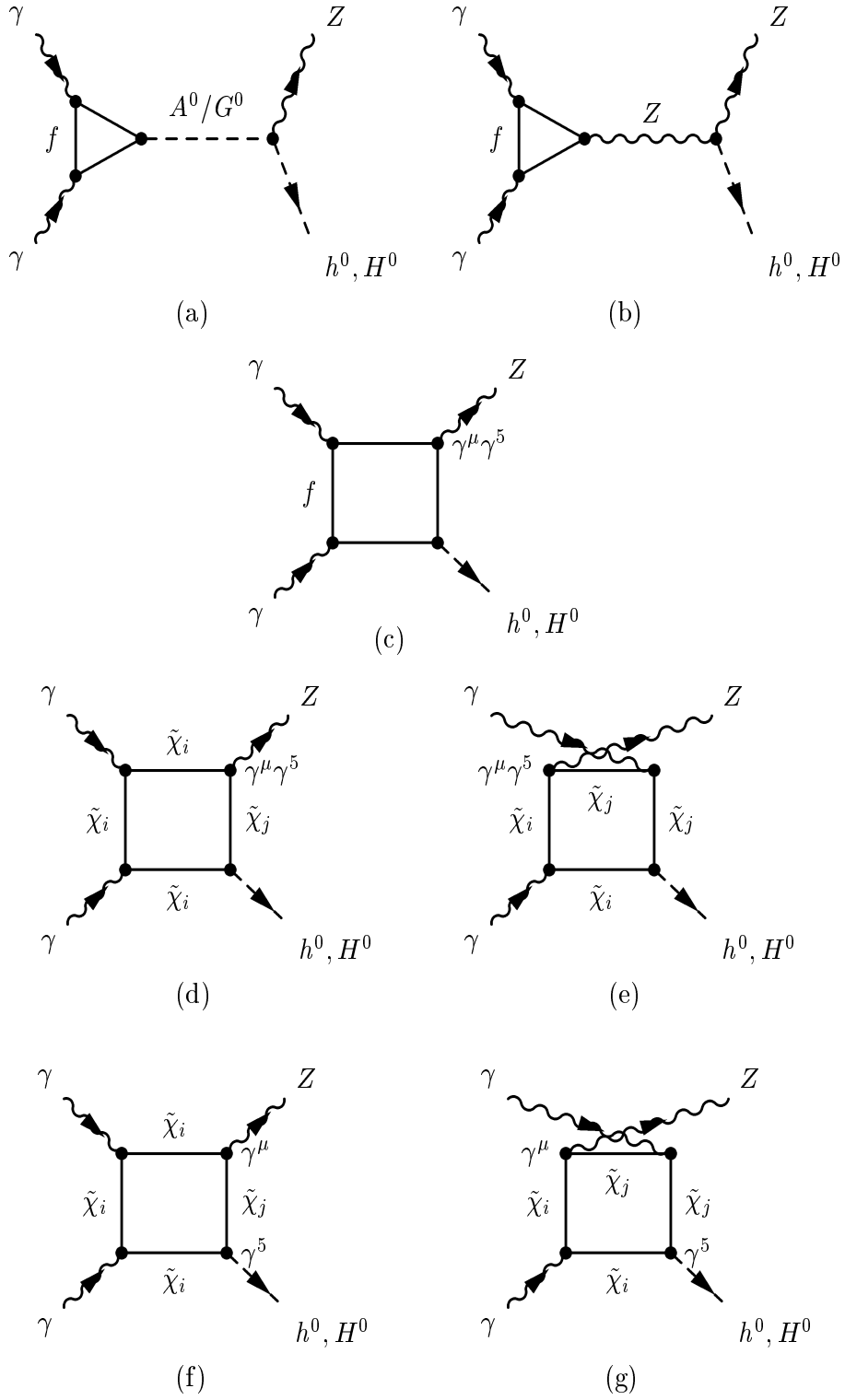


Figure 1: Generic diagrams describing the various contributions to  $\gamma\gamma \rightarrow Zh^0, ZH^0$  in SUSY models. Solid lines correspond to fermions, broken lines to scalars, while wavy lines correspond to gauge bosons. Similar diagrams also describe the Standard Model. The diagrams in (d-g) for  $j \neq i$  describe the mixed chargino boxes.

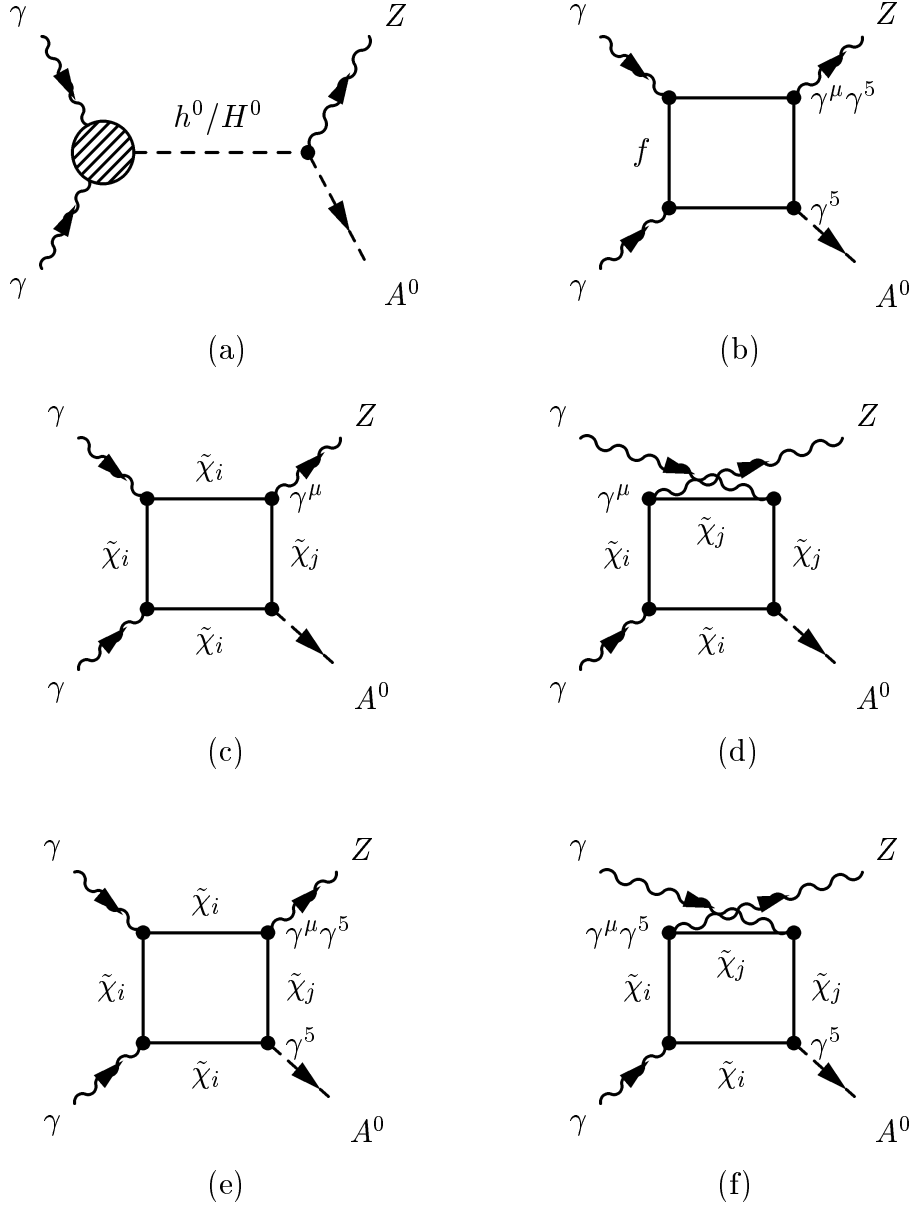


Figure 2: Generic diagrams describing the various contributions to the  $\gamma\gamma \rightarrow ZA^0$  in SUSY models. Solid lines correspond to fermions, broken ones to scalars, while wavy lines correspond to gauge bosons. The diagrams in (c-f) for  $j \neq i$  describe the mixed chargino boxes.

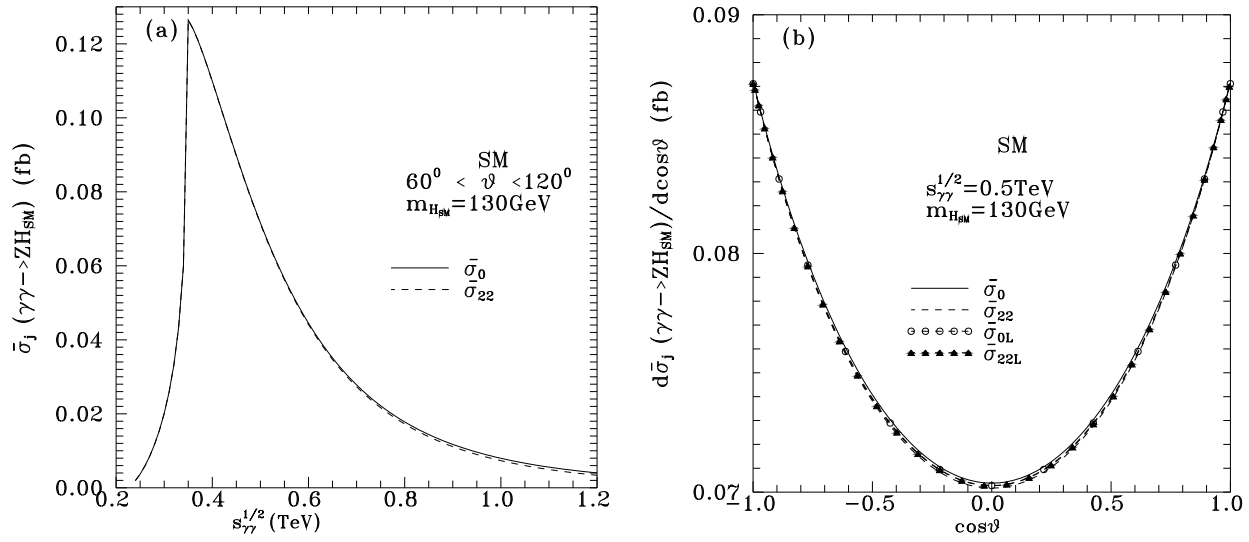


Figure 3:  $\gamma\gamma \rightarrow ZH$  cross sections in SM. The cross sections  $\bar{\sigma}_{0L}$  and  $\bar{\sigma}_{22L}$  refer to the production of longitudinal  $Z$  bosons.

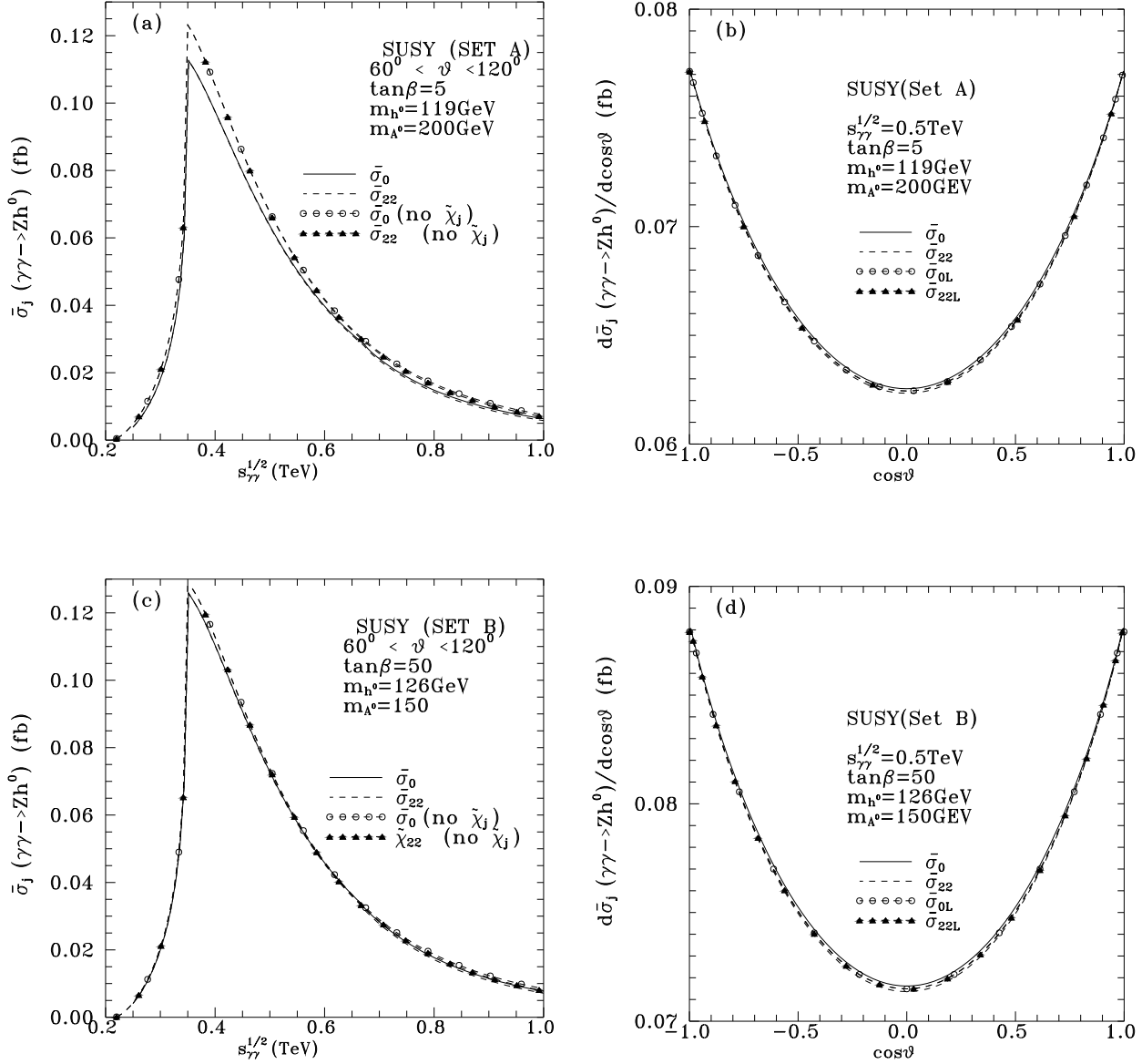


Figure 4:  $\gamma\gamma \rightarrow Zh^0$  cross sections in SUSY. The complete list of the parameters used in sets A and B appear in Table 1. The label (no  $\tilde{\chi}_j$ ) means that the chargino contribution has been suppressed in the computation of the cross section.

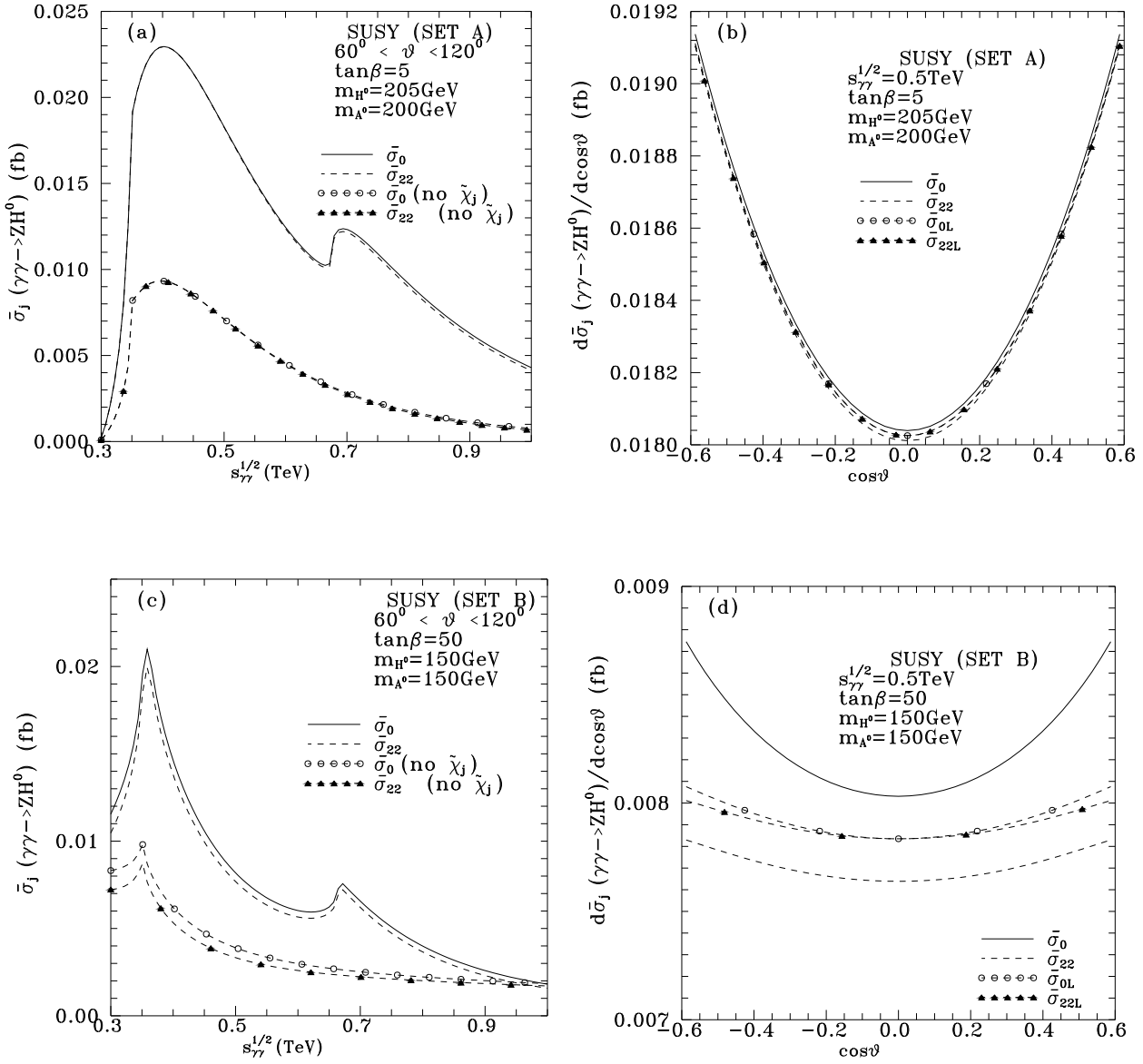


Figure 5:  $\gamma\gamma \rightarrow ZH^0$  cross sections in SUSY. The complete list of the parameters used appear in Table 1. Same captions as in Fig.3,4.



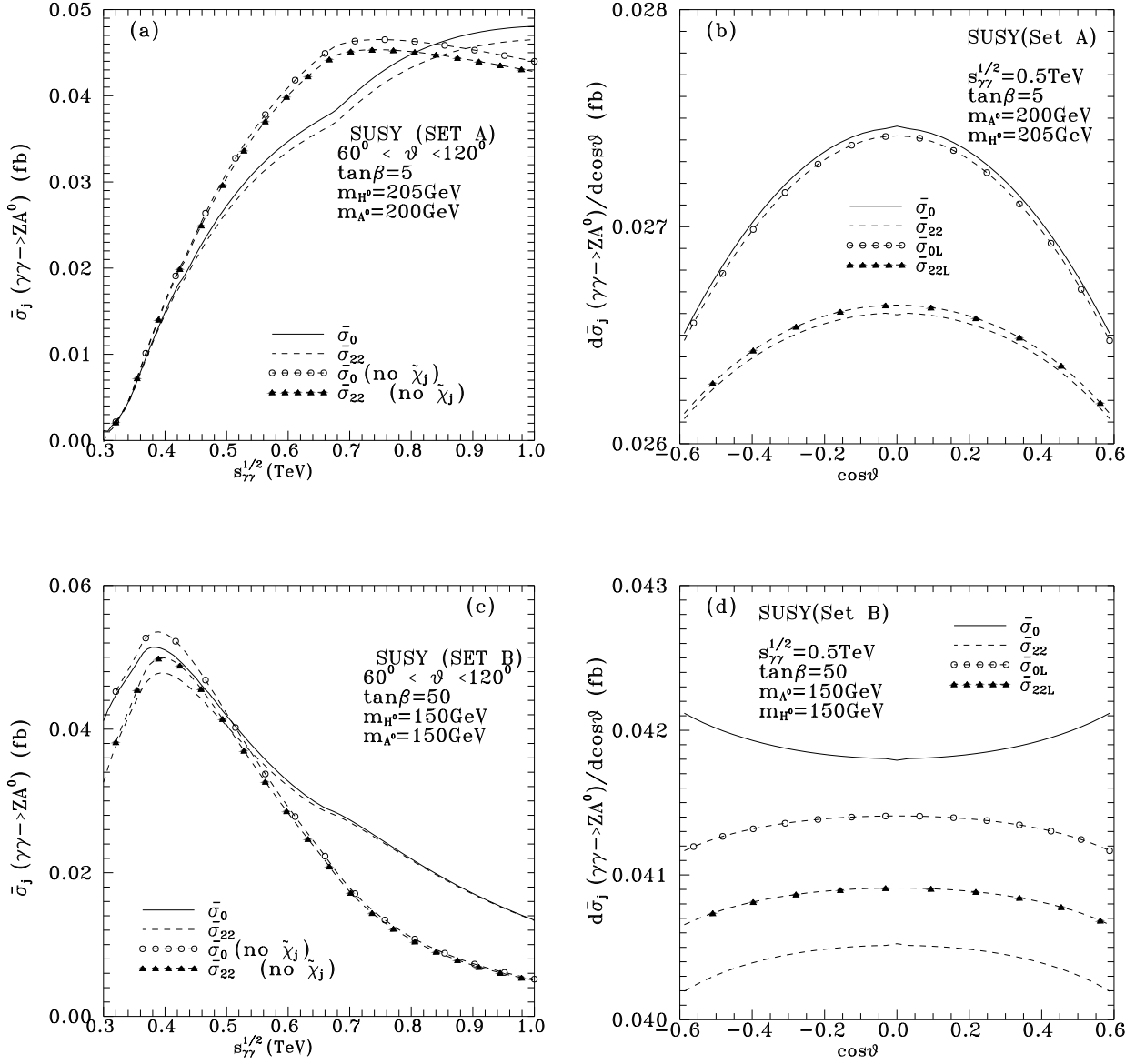


Figure 6:  $\gamma\gamma \rightarrow ZA^0$  cross sections in SUSY. The complete list of the parameters used appear in Table 1. Same captions as in Fig.3,4.